63-4.1

NAVWEPS REPORT 8354
NOTS TP 3241
COPY 52

DESCRIPTION OF A CONTROL SYSTEM FOR ROCKET-MOTOR MASS MEASUREMENT

by

R. A. Elston
Test Department

ABSTRACT. A technique for determining the mass of large rocket motors during burning, and an experimental system developed for use with the NOTS-designed three-component static-test stand at the Skytop facility, are described. The technique involves mounting the rocket motor on springs and continuously exciting the spring-mass system at its natural frequency.

The theoretical design of the control system is discussed and theoretical system-performance characteristics are compared with those of the experimental system. Results of an analog simulation study conducted in two degrees of freedom are included in the appendix.

Analysis of data from an evaluation test involving the static firing of a large rocket motor, indicates that a 2% accuracy in mass measurement is attainable with the experimental system. Criteria for the design of an operational system that will produce an accuracy of 1% are presented.

U.S. NAVAL ORDNANCE TEST STATION
China Lake, California
June 1963

U. S. NAVAL ORDNANCE TEST STATION

AN ACTIVITY OF THE BUREAU OF NAVAL WEAPONS

C. BLENMAN, JR., CAPT., USN
Commander

WM. B. MCLEAN, PH.D.
Technical Director

FOREWORD

In the static testing of rocket motors, the prime requirement is to be able to determine accurately the force of the developed thrust. With the advent of large rocket motors it became necessary to test them with correspondingly large static-test stands having very low natural frequencies. However, because of the low-frequency characteristics of the test stand, oscillations occurred during irregular burning, thrust buildup, and termination periods and these extraneous oscillations were recorded as part of the thrust load-cell data. To separate oscillation-caused data from the thrust data, a data combination system was developed. To use the system it is necessary to know the mass of the oscillating system throughout rocket-motor burning.

This report, issued at the working level, describes a technique for determining the mass of a system continuously during rocket-motor burning. It also includes a description of the theoretical development of an experimental mass-measuring system, the design and evaluation of a prototype system, results of an analog simulation study, and information on full-scale testing.

This project was started in the spring of 1959 under Task Assignment SP 71401-7 and was completed with an evaluation firing in December 1962 under Task Assignment SP 71402-8. The report has been reviewed for technical accuracy by Benjamin Glatt, R. W. Murphy, D. P. Ankeney, and C. E. Woods.

R. A. APPLETON
Head, Range Division

Released under
the authority of
IVAR E. HIGHBERG
Head, Test Department

NOTS Technical Publication 3241
NAVWEPS Report 8354

Published by . . . . . Test Department
Manuscript 30/MS-579
Collation. . . . . .Cover, 36 leaves, abstract cards
First printing . . . . . 285 numbered copies

CONTENTS

Figures:

ACKNOWLEDGMENT

The initial discussions on this mass-measuring technique were coordinated by H. S. Olson, D. Nelson, and D. P. Ankeney. The author is indebted to them for their technical and managerial assistance in resolving some of the initial problems encountered and for their continued support throughout the development of this technique.

Further acknowledgment is made of the many other individuals, especially those in the Design and Development Branch of the Test Department, for their direct support in the basic design of the experimental system and for their conscientious efforts in helping to carry the development through to the successful completion of the evaluation test.

INTRODUCTION

In the static testing of large rocket motors, early test stands often employed a standard load cell to solve the following simplified thrust equation:

$$T = KX \tag{1}$$

where

T = thrust
K = spring constant of load cell
X = spring displacement

It soon became apparent, however, that the necessarily low resonant-translation frequency generally associated with large-scale testing resulted in the occurrence of undesirable oscillations or 'ringing' during thrust buildup and thrust termination. This is the result of the thrust buildup and termination appearing as approximate step inputs to an underdamped stand load-cell system. To account for these oscillations, the basic single degree of freedom equation can be used.

Consider the rocket motor and stand illustrated in Fig. 1

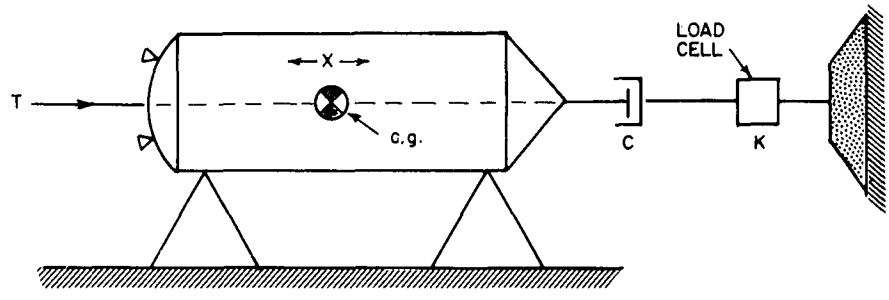

FIG. 1. Rocket Motor and Thrust Stand Schematic Illustrating Basic Thrust Equation.

Where:

T = developed thrust, lb

K = spring constant of load-cell, lb/ft

C = lumped damping constant, $\frac{\text{lb-sec}}{\text{ft}}$

$M(t)$ = mass of total moving structure (varies with time), $\frac{\text{lb-sec}^2}{\text{ft}}$

c.g. = center of gravity location (assumed fixed throughout burning)

X = displacement of mass center of gravity

By summing the forces along the translational axis the following equation is obtained:

$$T = KX + C\dot{X} + M(t)\ddot{X} \qquad (2)$$

It is noted that this basic equation is a differential equation of the second order. As such, with the damping constant C relatively small (as it should be for accurate determination of thrust buildup and termination), a step input or sudden change in thrust will result in large overshoots and relatively undamped oscillations in X. These oscillations are recorded as part of the load-cell data and, because of their low-frequency, they cannot be filtered without sacrificing data resolution. As a solution to this problem NOTS has considered the development of a data-combination system which enables the separation of these oscillations from the load-cell data.* With this system, data from an accelerometer mounted with its sensitive axis along the rocket-motor line of thrust will be combined with the standard load-cell data and, by assuming a linear change in rocket mass during burning (as determined by weighing the rocket motor before and after burning or as calculated from internal ballistics data) the basic thrust equation can be solved. The accelerometer data is integrated to obtain $\dot{X}$ and by estimating C the second term of Eq. (2) can also be included.

While in many routine tests the assumption of a linear change in mass during burning might be useful in applying accelerometer data to obtain accurate thrust determinations, it is not adequate for use with

*U. S. Naval Ordnance Test Station. A System for Correcting for Spurious Natural-Frequency Ringing of Rocket Static Thrust Stands, by J. S. Ward. China Lake, Calif., NOTS, 1 September 1960. (NAVWEPS Report 7569, NOTS TP 2541).

propulsion systems in which the propellant mass-burning rate, intentionally or otherwise, deviates seriously from a constant value during burning. Furthermore, it is often desirable to know the mass-burning rate to the same degree of accuracy as that of the thrust at all times during burning in order to evaluate the changing effects of erosive burning, combustion-chamber free volume, operating pressure, charge deformation, specific thrust, nozzle erosion, propellant composition, etc. Likewise, it is very important to have continuous mass measurement in case of mechanical failure in the propulsion system since only limited specific thrust and specific impulse data can be obtained from an incomplete test if the mechanical condition of the nozzle and the amount of propellant burned prior to the failure are not known.

In reviewing this problem it was judged that a reasonably sophisticated evaluation of test records would provide a significant increase in information if a system could be devised for determining rocket mass continuously during a firing. With the high cost of testing large motors, this increased information would create substantial savings in both time and money during developmental programs.

Two methods which have been used for determining the mass of a burning rocket motor are referred to as the Z Load Cell Method and internal ballistics or Pressure Method.

The Z Load Cell Method involves the use of load cells in the thrust stand legs to measure the vertical force during burning. If the stand and thrust misalignments are known and assumed constant throughout burning, a determination of mass versus time can be made. The overall accuracy in mass determination is estimated as 5%; however, it is felt that improved stand alignments and data reduction techniques may improve this figure. Continued investigation into this method is planned.

To use the Pressure Method of determining mass requires that the rocket motor chamber pressure be known throughout burning. It is also necessary to know the total amount of propellant burned and the throat area of the nozzle. Using these parameters, calculations of mass burning rates are made. It has been estimated that, due to the difficulty in measuring these parameters and the linearizing assumptions made in converting the information to mass-burning rates, an accuracy of 5% is the best attainable with this technique, too.

Using this as a general guideline in determining the feasibility and usefulness of a particular system, the following technique for the continuous measurement of mass has been developed. The horizontal NOTS Model II thrust stand used in Bay I at Skytop (Fig. 2) was selected for system development,* since it lends itself favorably to this technique of mass measurement and since considerable knowledge had been gained of its operational characteristics.

*The NOTS Model II thrust stand was designed with a six-compoment capability but was used as a three-component stand for this development.

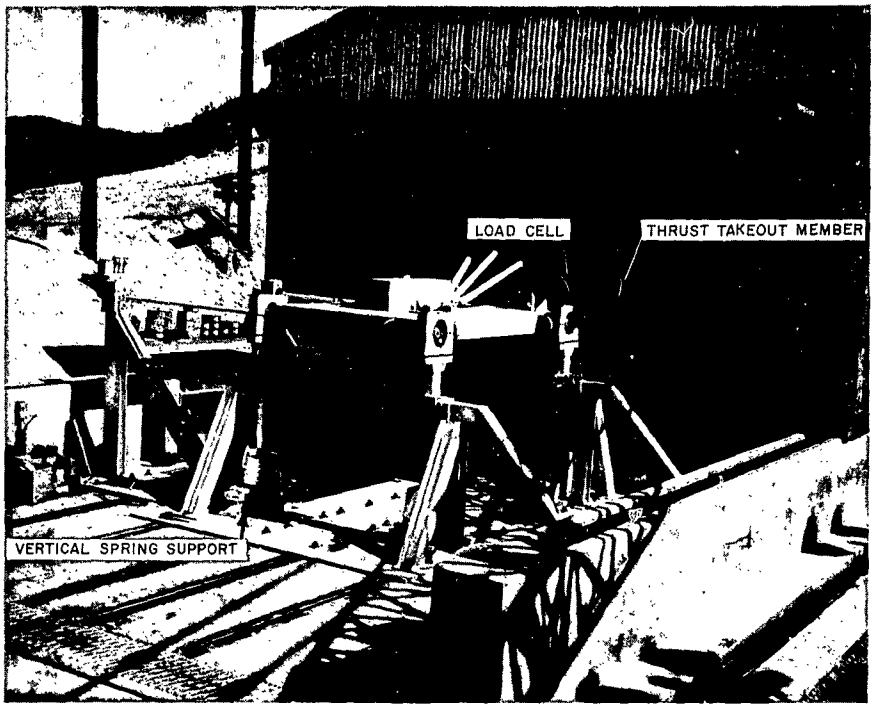

FIG. 2. NOTS Model II Thrust Stand With Dummy Load.

An evaluation test of the experimental system and an analog simulation study have been conducted. The evaluation test is discussed on page 35; results of the analog simulation study are given in Appendix A; the derivation of analog simulation equations is presented in Appendix B; Appendix C includes the derivation of system transfer functions.

MASS MEASUREMENT TECHNIQUE

The mass of a burning rocket motor is determined by continuously exciting the rocket-motor-stand system at its undamped natural frequency when supported on springs as shown schematically in Fig. 3. If the vibrating system is assumed to have a single degree of freedom and slowly varying mass then the mass can be calculated throughout burning from the following equation:

$$M(t) = \frac{K}{\omega_{n(t)}^2} \qquad (3)$$

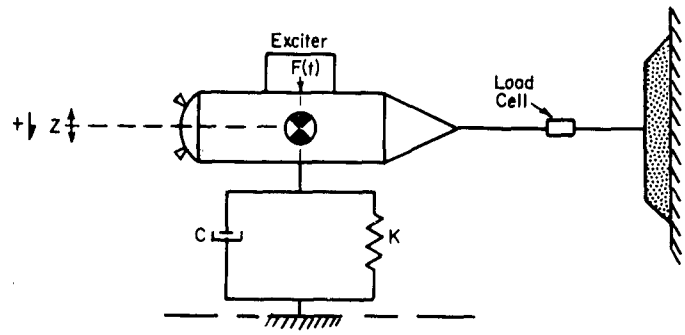

FIG. 3. Rocket Motor and Thrust Stand Schematic.

where

$\omega_{n(t)}$ = undamped natural frequency of vibrating system (variable with burning time)

$F(t) = F_o \sin\omega t$ (sinusoidal force generator), lb

$M(t)$ = effective vibrating mass, $\frac{\text{lb-sec}^2}{\text{ft}}$

K = lumped spring constant, lb/ft

C = lumped damping constant, $\frac{\text{lb-sec}}{\text{ft}}$

Z = vertical displacement of rocket motor center of gravity, ft

This equation is derived in writing the dynamic equation of motion. Applying Newton's second law to the system of Fig. 3 and assuming a non-changing mass environment, the differential equation of translational motion is written:

$$F_o \sin\omega t = M \frac{d^2Z}{dt^2} + C \frac{dz}{dt} + KZ \tag{4}$$

Applying the LaPlace transform operator, S

$$\frac{F_o \omega}{S^2 + \omega^2} = S^2 MZ_{(S)} + SCZ_{(S)} + KZ_{(S)} \tag{5}$$

solving for $Z_{(S)}$

$$Z_{(S)} = \frac{F_o \omega}{(S^2 + \omega^2)} \quad \frac{1}{(S^2 M + SC + K)} \tag{6}$$

rearranging

$$Z_{(S)} = \frac{F_o \omega}{M(S^2 + \omega^2)} \quad \frac{1}{(S^2 + S\frac{C}{M} + \frac{K}{M})} \tag{7}$$

By definition, any linear second-order differential equation can be written in terms of two quantities: ζ and ω_n.

The damping ratio ζ is the ratio of the damping that exists in a second-order system to the critical damping; i.e., the value of damping resulting in a nonoscillatory response following a step input. The undamped natural frequency ω_n is the frequency of oscillation that occurs for zero damping. By definition, then

$$2\zeta\omega_n = \frac{C}{M} \tag{8}$$

$$\omega_n^2 = \frac{K}{M} \tag{9}$$

Rearranging, Eq. (9) then becomes original Eq. (3):

$$M = \frac{K}{\omega_n^2}$$

Substitution of Eqs. (8) and (9) in Eq. (7) yields

$$Z_{(S)} = \frac{F_o \omega}{M(S^2 + \omega^2)} \quad \frac{1}{(S^2 + 2\zeta\omega_n S + \omega_n^2)} \tag{10}$$

Rearranging

$$Z(S) = \frac{F_o \omega}{M(S^2 + \omega^2)} \qquad \frac{1}{[(S + \zeta\omega_n)^2 + \omega_n^2 (1 - \zeta^2)]} \tag{11}$$

Using the appropriate transform function,* the complete solution of the displacement of the rocket motor is found to be:

$$Z(t) = \frac{F_o \omega}{M(\omega_n^4+\omega^4-2\omega_n^2\omega^2+4\zeta^2\omega_n^2\omega^2)^{\frac{1}{2}}}\left[\frac{1}{\omega}\sin(\omega t-\theta_1)+ \frac{\epsilon^{-\zeta\omega_n t}\sin(\omega_n\sqrt{1-\zeta^2}-\theta_2)}{\omega_n\sqrt{1-\zeta^2}}\right] \tag{12}$$

where

$$\theta_1 \triangleq \tan^{-1}\left(\frac{2\zeta\omega_n\omega}{\omega_n^2 - \omega^2}\right) \quad ; \quad \theta_2 \triangleq \left(\frac{-2\zeta\,\omega_n^2\sqrt{1 - \zeta^2}}{2\zeta^2\omega_n^2 - \omega_n^2 + \omega^2}\right)$$

Considering only the steady-state solution it can be seen that as the frequency of the exciting force ω approaches the undamped natural frequency ω_n, the phase angle θ_1 approaches 90°. In other words, when the spring-mass system is oscillating at the undamped natural frequency the displacement Z lags the exciting force in phase by 90° so that

for

$$F(t) = F_o \sin\omega t \tag{13}$$

$$Z(t) = \frac{F_o}{2M\,\zeta\omega_n^2}\sin(\omega t - 90°) \tag{14}$$

The problem remaining, then, is to design a control system to maintain this 90° phase relationship continuously throughout burning. By maintaining this relationship, system oscillation at the undamped natural frequency is insured and computations of mass versus burning time can be made by using Eq. (3).

*Gardner, Murray F. and John L. Barnes. Transients in Linear Systems, Vol. 1. New York, Wiley, 1956. Transform pair 1.357, Appendix A.

EXPERIMENTAL SYSTEM

PHASE DETERMINATION

The first step in the design of the control system was to devise a method of sensing the phase relationship of the sinusoidal-force generator exciting function F(t) with that of the spring-supported rocket-motor stand system displacement function Z(t).

The waveforms in Fig. 4a, which depict the phase relationship between these two functions at an instant in time when the spring-mass system is oscillating just below the undamped natural frequency, show a phase angle of 80°. In order to detect the phase polarity (i.e., lead or lag, in reference to the desired 90° value) a third waveform is added. This waveform, shown in Fig. 4b, is always leading the exciting function by 90°. For the condition shown (i.e., for the system oscillating below the undamped natural frequency) it is now possible to write logic equations relating the three waveforms and the 10° phase error.

Using Boolean Algebra terminology and selecting A, B, C to represent positive and $\overline{A}$, $\overline{B}$, $\overline{C}$ to represent negative values, the following equations are written:

$$\overline{A}\ \overline{B}\ \overline{C} = 1 \qquad (15)$$

$$A\ B\ C = 1 \qquad (16)$$

where A B C is defined as A and B and C.

In the same manner it is possible to write the logic equations for the condition wherein the spring-mass system is oscillating above the undamped natural frequency. As illustrated in Fig. 4c, the logic equations are:

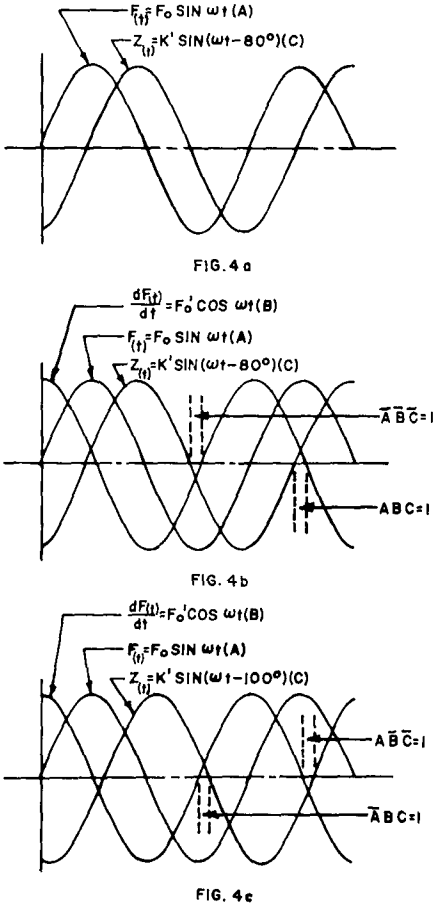

FIG. 4. Phase Comparator Logic.

$$\bar{A}\,B\,C = 1 \tag{17}$$

$$A\,\bar{B}\,\bar{C} = 1 \tag{18}$$

These equations were used in designing the diode logic circuitry (phase comparator), a schematic diagram of which appears in Appendix C. The phase comparator generates an error pulse of constant amplitude with the width equal to the relative phase error. The pulse is positive for a system-oscillation frequency below the undamped natural frequency and negative for frequencies above the undamped natural frequency. Since one of the four logic equations will be satisfied at each crossover of the displacement wave, a digital sensor exists with a sampling rate of two samples per cycle. This low sampling rate in a closed-loop system will tend to increase system-response time which will generally degrade system performance. In this experimental system, however, the power train has a time constant of approximately 200 millisec and the additional lag introduced by the lowest sampling rate of 20 samples per second does not appear to be significant. It is apparent that in the design of fully operational systems having power train-time constants considerably lower than 200 millisec, techniques for increasing the digital sampling rate will have to be devised.

FORCE GENERATOR

The force generator is a mechanical device consisting of two sets of eccentric weights connected through a differential. The arrangement and relative rotation of the weights is shown in Fig. 5.

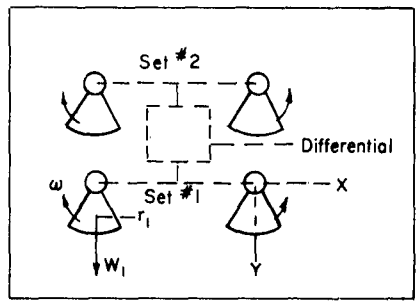

FIG. 5. Rotating Eccentric Weights. Arrows indicate direction of rotation.

With an individual eccentric weight W_1, a radius of rotation r_1 and an angular velocity ω, the centrifugal inertia force is given by

$$F_1 = \frac{W_1}{g} \omega^2 r_1 \tag{19}$$

where

F_1 = force, lb
W_1 = effective weight, lb
r_1 = radius of rotation, ft
g = gravitational force, 32.2 ft/sec^2
ω = angular velocity, rad/sec

Since the two weights of each set are coupled together and rotate in opposite directions, the centrifugal inertia force along the x axis is canceled out and a force is generated only along the y axis. The force is sinusoidal and has a maximum magnitude which is dependent on the phase relationship between the two sets of weights. Thus, the excitation force is calculated using the following equation:

$$F_1 = \frac{4 W_1}{g} r_1 \omega^2 \sin(\theta_1 - \theta_2) \sin\omega t \tag{20}$$

The desired magnitude of force can be generated by selecting the proper phase angle between the two sets of weights with the differential; hence the term $\sin(\theta_1 - \theta_2)$.

The magnitude of the force necessary to excite the spring-mass system at the undamped natural frequency is dependent upon: (1) the acceleration limitations in the vertical plane of the rocket motor under test, (2) the damping existing in the spring-mass system, and (3) the mass of the vibrating system. For the rocket motor and stand assembly being tested, the following specifications apply:

Sprung weight with live rocket motor (propellant unburned) in stand	25,000 lb
Sprung weight with rocket-motor carcass (propellant burned) in stand	10,000 lb
Effective spring constant	3.72×10^6 lb/ft
Undamped natural frequency (live motor in stand)	10.88 cps*
Undamped natural frequency (motor carcass in stand)	16.88 cps*
Damping ratio ζ (this ratio was calculated using Eq. (22) and estimating F_o, while maintaining a 1-g acceleration)	0.01 or 1%
Maximum vertical acceleration	1.0 g
Burning time	60 sec

By taking the second derivative of Eq. (14), the following expression is obtained for the acceleration of the spring-mass system oscillating at the undamped natural frequency:

$$\ddot{Z}_{(t)} = \frac{F_o}{2M\zeta} \cos\omega t \tag{21}$$

The vibrating structure (including a first-stage rocket motor) has a mass of approximately 720 slugs when the rocket motor propellant is unburned and approximately 320 slugs with the rocket motor carcass. The damping ratio is small since dash pots have not been added and the only damping present (such as propellant flexibility) is that which is inherent in the system. ζ is estimated at approximately 0.01. Under these conditions, the magnitude of the exciting force can be computed from Eq. (21).

Maximum acceleration occurs when $\cos\omega t = 1$. Therefore, rewriting Eq. (21)

$$F_o = 2\zeta M\ddot{Z} \tag{22}$$

*Values determined experimentally.

and for the conditions above

$$F_o = (2)(0.01)(320)(32.2) = 206 \text{ lb} \tag{23}$$

This value of F_o will result in a 1-g acceleration with a rocket motor carcass mounted in the stand. Since ζ is considered constant throughout burning, it is apparent that a much larger exciting force could be tolerated under live motor conditions. However, since the force generator differential will not be operated during the test, it is necessary to restrict the maximum force to that indicated in Eq. (23).

It is now possible to calculate the maximum horsepower required to drive the force generator. The power required in the system is the sum of the power needed to provide angular acceleration; to overcome damping in the spring-mass system, shaker, and drive motor, to counteract the losses in the gear train; and to compensate for torque feedback due to the oscillatory motion of the shaker in relation to the drive motor. The maximum horsepower requirement is calculated by:

$$T = J\ddot{\theta} + B\dot{\theta} \text{ (unknown)} + T_f + \text{gear train losses (unknown)} + \text{spring-mass damping} \tag{24}$$

and

$$T_f = m\ell \left[\ell\ddot{\theta} + (\ddot{Z} + Z\dot{\theta}^2) \cos\theta + Z\ddot{\theta} \sin\theta\right] \tag{25}$$

where

T = total torque reflected into the drive motor, lb-ft

T_f = feedback torque, lb-ft

$\dot{\theta}$ = angular velocity, rad/sec

$\ddot{\theta}$ = angular acceleration, rad/sec^2

$m\ell$ = effective shaker unbalance, lb-sec^2

ℓ = effective mass lever arm, ft

J = effective system inertia, lb-ft-sec^2

The derivation of Eq. (25) is given in Appendix B.

To calculate the maximum power required, $\dot{\theta}$ and $\ddot{\theta}$ will be assumed to occur simultaneously and have the following values:

$\dot{\theta}$ max = 106 rad/sec

$\ddot{\theta}$ max = 10 rad/sec^2

The term $\dot{\theta}$ is based on the system being in operation with a rocket motor carcass in the stand and $\ddot{\theta}$ is based on the maximum transient response requirement as indicated in the figure shown on page 30.

Since the second and third terms of Eq. (25) have a 90° relationship, only the second term need be considered to obtain peak torque. When $\cos\theta = 1$, this equation becomes

$$T_f = m\ell\ (\ell\ddot{\theta} + \ddot{Z} + Z\dot{\theta}^2) \qquad (26)$$

where

$$m\ell = 0.02$$

$$\ell = 0.096$$

then

$$T_f = (0.02)(0.096 \times 10 + 32.2 + 0.00287 \times 106^2) = 2.60 \text{ lb-ft}$$

The additional torque required to provide the desired acceleration is

$$J\ddot{\theta} = (10)(0.71) = 7.1 \text{ lb-ft}$$

where

$$J = 0.71$$

Then

$$T = T_f + J\ddot{\theta} = 2.60 + 7.1 = 9.7 \text{ lb-ft total known torque}$$

The horsepower transmitted by a shaft making n revolutions per minute under a torque of T lb-ft is

$$HP = \frac{2\pi n\ T}{33,000} \tag{27}$$

$$HP = \frac{(2\pi)(16.88)(60)(9.7)}{33,000} = 1.87$$

The horsepower requirement to provide acceleration and to compensate for torque feedback then, is 1.87. The additional power requirement to overcome spring-mass damping is obtained from the following power equation, where $\dot{Z}$ is the velocity of the displacement Z and C is the damping constant as in Eq. (2):

$$\text{Power} = \dot{Z}^2 C \tag{28}$$

The damping C as determined from Eq. (8) is 680 $\frac{\text{lb-sec}}{\text{ft}}$ and displacement velocity $\dot{Z}$ is obtained by differentiating Eq. (14); therefore,

$$\text{Power} = (0.304)^2(680) = 63\ \frac{\text{lb-ft}}{\text{sec}}$$

$$HP = \frac{63}{550} = 0.12$$

This results in a total known instantaneous peak power requirement of approximately two horsepower. A drive motor is normally selected by considering both the instantaneous and average power requirements. In this case, however, the average power dissipated, other than that due to damping, is difficult to ascertain analytically. It has been determined experimentally that the average power dissipated is approximately one horsepower. It appears, therefore, that the selection of the 5-horsepower motor used in this experiment is somewhat conservative and that improved response could be realized by carefully selecting a motor just matching the power requirements.

SYSTEM ANALYSIS

The block diagram of Fig. 6 represents the complete experimental control system when it is operating as a relay type with sampling. The system was initially constructed as a straight sampling type (i.e., as shown in Fig. 6, without the flip-flop). Using the sampled data system, a rocket-motor firing was conducted; the results are discussed later in this report. The system performed satisfactorily; however, in preparation for a second evaluation test it was found that the addition of the flip-flop improved system performance. (It was planned to conduct the second test using the configuration shown in Fig. 6; however, this test could not be conducted because of a rocket motor malfunction which partially destroyed the drive motor and shaker.)

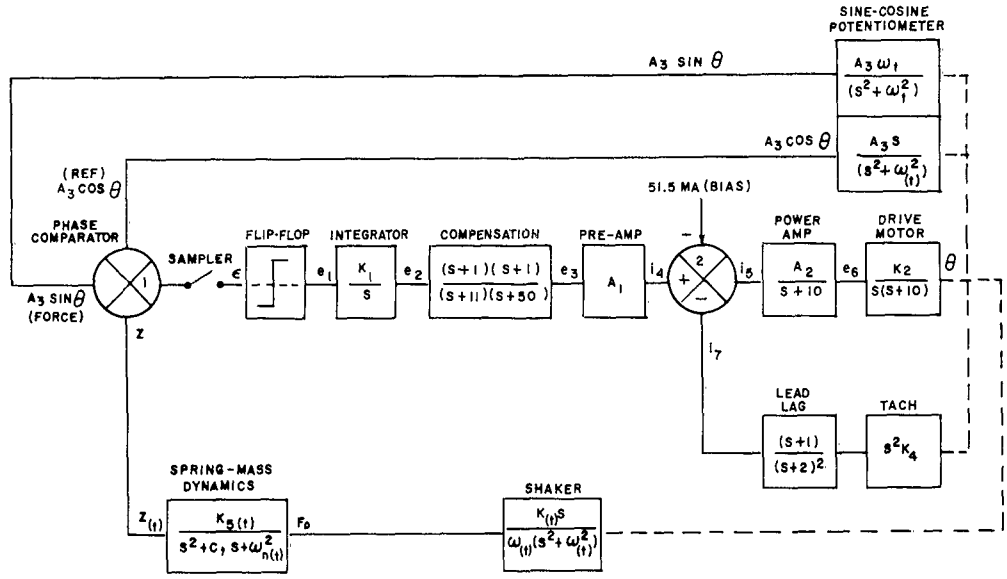

FIG. 6. Block Diagram of the Experimentally Tuned Control System.

Although the evaluation test was conducted with the system operating as a straight sampling type, it is felt that significant improvement in closed-loop performance was obtained with the addition of the flip-flop and that the analysis should be made for the relay sampling type system. No recorded data of the relay-sampling system were obtained because of the rocket-motor malfunction. The system was operated, however, with a rocket-motor carcass in the stand prior to this catastrophe and the system performance was observed. The significant performance characteristics are indicated for comparison on the response curves obtained with the straight sampling system.

In Fig. 6, comparator No. 1 and the 'sampler' represent the phase comparator described previously. The phase of the waveform θ, representing the exciting force is compared with the phase of the waveform Z representing the displacement of the oscillating spring-mass system. A sampling rate of two samples per cycle has been established. The output of the sampler is used to trigger a flip-flop which in turn is used as the error signal for integration. (At least one stage of integration in addition to that performed by the drive motor is desirable in velocity control since this results in a Type 2 system which exhibits a zero steady-state error in a simple configuration--i.e., a single loop with continuous feedback. A theoretical derivation is given in Chapter 7 of Servomechanism Analysis.*) The addition of the flip-flop changes the servomechanism from a straight sampling type to a relay type with sampling.

Usually, the performance characteristics of relay servos are not particularly favorable; that is, a servo with continuous (proportional) feedback will generally out-perform the relay type. In this case, however, where it is necessary to compare the phase relationship of two sinusoidal waveforms (one of which has a variable amplitude), a practical device for comparing the phase relationship continuously is not readily available. The phase comparator thus uses diode logic circuitry to produce pulses which are phase dependent at each zero crossover of the displacement waveform. The pulses are of constant amplitude but have a width directly proportional to phase error.

Comparing the system performance during experimental operation, both as a straight sampling type and as a relay type with sampling, it was found that the relay type exhibited superior characteristics. With the relay configuration, it was possible to more-than-double the forward-loop gain of the control system with a consequent improvement in frequency response. The steady-state oscillation or limit cycle of the servo system was more pronounced when operated as a relay type; however, the frequency of oscillation was higher, and better response was obtained for small step inputs in phase error. It should be noted, however, that with the use of highly sophisticated compensating circuitry, a straight sampling system performance, comparable to that of the relay type, could very likely be obtained. The compensating circuitry necessary to attain this result is quite complex making experimental improvement of closed-loop system performance extremely difficult. While on the other hand, the relay system required relatively elementary compensating circuitry and produced the desired result.

From the control system diagrammed in Fig. 6, it is apparent that several nonlinearities exist. (A component is said to be nonlinear if the equations describing its dynamics contain terms made up of the product or quotient of a dependent variable and a time variant coefficient.) The equation describing the spring-mass dynamics is written:

*Thaler, G. J. and R. G. Brown. Servomechanism Analysis. New York, McGraw-Hill, 1953.

$$F_o\left(\frac{d\theta}{dt}\right)^2 \sin\omega_{(t)}t = M_{(t)} \frac{d^2Z}{dt^2} + C \frac{dZ}{dt} + KZ \qquad (29)$$

Since this equation is of the nonlinear type, it cannot be handled by regular LaPlace methods.

The complete solution of the nonlinear system will not be attempted, only the two end points of operation will be considered. That is, the control system will be analyzed operating first in a nonchanging mass environment with a rocket motor carcass and then with a live rocket motor mounted in the thrust stand. To simplify and linearize the system, the spring-mass dynamics will be considered analogous to a low-pass filter. That is, the spring-mass system will be considered to introduce phase lag and amplitude attenuation in the feedback loop. Data obtained with the experimental system and in the analog simulation studies (Appendix A), indicate that a lag in the spring-mass system to simulated step inputs exists and that the response curve approaches that of an exponential.

This lag characteristic is described in some detail in NAVWEPS Report 7741* which illustrates that a step change in mass will result in an exponentially rising input error to the control system. The assumption has been made here that this lag will also appear when changes in driving-function frequency are experienced and that this lag is in the feedback path. This assumption is open to considerable discussion; however, it is shown that, with this assumption, reasonable agreement with experimental data can be obtained. Using the experimentally determined time constants, the following transfer functions will be used to simulate the spring-mass system in the analysis of the two end points of operation:

with a rocket motor carcass in the stand

$$\frac{Z}{\theta} = \frac{3}{S + 3} \qquad (30)$$

with a live rocket motor in the stand

$$\frac{Z}{\theta} = \frac{2}{S + 2} \qquad (31)$$

This simplifies the system block diagram to that of Fig. 7.

*U. S. Naval Ordnance Test Station. Determination of Rocket-Motor Mass by Measurement of the Natural Frequency of a Mass-Spring System, by Benjamin Glatt. China Lake, Calif., NOTS, 15 June 1961. (NAVWEPS Report 7741, NOTS TP 2706).

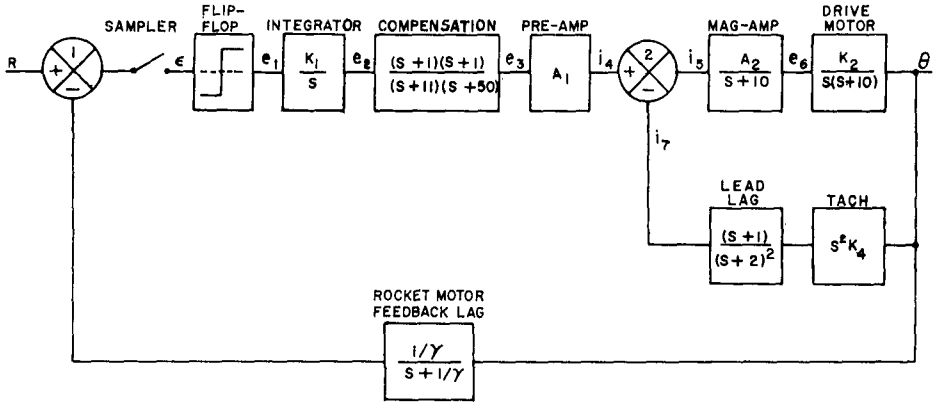

FIG. 7. Simplified Block Diagram of the Compensated Control System.

It should be pointed out that these time constants may be in considerable error. As noted in NAVWEPS Report 7741, the time constants are dependent on the damping and mass of the system at the time the step change in mass is initiated. The experimental data were obtained by suddenly changing the driving-function frequency and observing the lag of the spring-mass system. Since, in this experiment, both the lag of the power train and the spring-mass system are combined, some error is evident in the interpolation. It is also noted that, although the time constant determined under live-motor conditions compares favorably with that of the analog study, there is a considerable difference between the time constant obtained under rocket-motor carcass conditions and that obtained in the analog study.

In the analog simulation, it was necessary to vary the damping with burning time and to distribute it unequally between front and rear supports to provide the needed coupling to cause pitching and thus reproduce the displacement curves obtained experimentally. It has since been determined under system operation that the structural oscillation of the thrust take-out member was also introducing pitching. It is evident, therefore, that the damping used in the analog study for the rocket-motor carcass condition is in error and that the time constant of the rocket-motor lag for this condition is also in error.

The speed of the shaker-drive motor is controlled by regulating the armature current while maintaining a constant field strength. The dynamic equations pertaining to this type of control are well developed.* The transfer function of the motor when driving an inertia load and neglecting frictional losses is:

*Thaler, G. J. and R. G. Brown. Op. cit., pp. 62-65.

$$\frac{\theta}{e_6} = \frac{\frac{K}{JR_a}}{S\left(S + \frac{K^2}{JR_a}\right)} \tag{32}$$

where

K = motor constant, $\frac{\text{ohm-sec}}{\text{rad}}$

R_a = motor armature resistance, ohms

J = total inertia load, ft-lb-sec^2

For the system under development, the motor constants K, and R_a were determined experimentally (Appendix C). The transfer function is:

$$\frac{\theta}{e_6} = \frac{K_2}{S(S + 10)} \tag{33}$$

The magnetic amplifier dynamic characteristics were also determined experimentally (Appendix C) and the transfer function is:

$$\frac{e_6}{i_5} = \frac{A_2}{(S + 10)} \tag{34}$$

Tachometer feedback is utilized in a minor loop. Since this is a velocity servo, the derivative of the tach or $\dot{\theta}$ is actually fed back and, since the tach output contains high-frequency components in the form of ripple, a filter is employed with the differentiator. The filter is connected in the feedback circuit of the operational amplifier used as the differentiator; filtering is accomplished since the gain becomes a function of frequency. The lead circuit is used to reshape the filter characteristics slightly and to allow optimization of the tach circuit under operating conditions. Derivation of the transfer functions appear in Appendix C.

The steady-state transfer function of the mag-amp and drive motor as a unit was obtained experimentally to determine if there were any nonlinearities in this portion of the control system. The curve plotted in Fig. 8 shows the nonlinearity that is present. If the mag-amp and drive-motor transient characteristics are considered not to change from the experimentally obtained values then the analysis of the end points of operation can continue by assuming an appropriate change in the forward loop gain as dictated by the curve in Fig. 8.

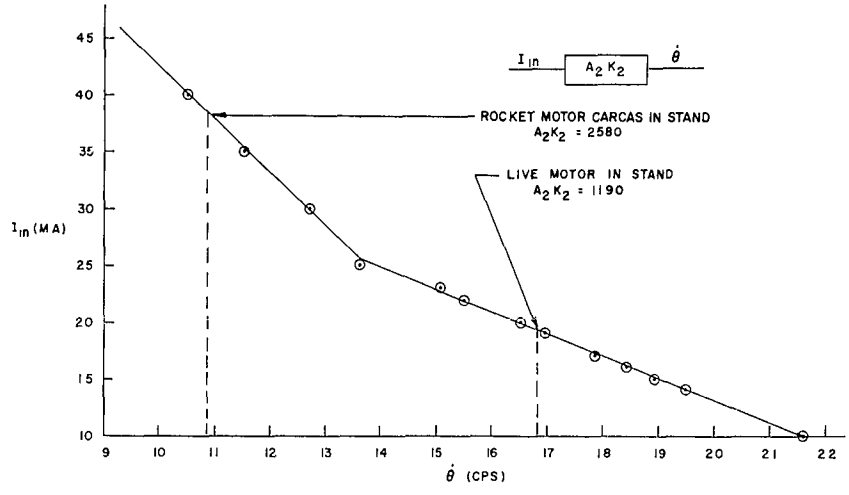

FIG. 8. Mag-Amp and Drive Motor Static Characteristics.

Under closed-loop operation it was observed that the control system exhibited a limit-cycle frequency of approximately one cycle per second. The sampling frequency at the low frequency end (with a live rocket motor mounted in the stand) is about 20 samples per second and about 36 samples per second at the high frequency end. Since the sampling rate is at least twenty times the switching rate of the relay (flip-flop), in this analysis the sampler will be considered to have an infinite frequency. That is, the error detector will be considered to be continuous.

The describing function technique for analysis of relay servos is particularly useful when relays approaching the ideal are used and when the system is of a high order.* A linear approximation is made in the frequency domain by defining a describing function in terms of the Fourier series for the component response to a sinusoidal input. With an ideal relay, the application of a sinusoidal input will result in a Fourier series describing the output consisting of the fundamental input and all odd harmonics thereof. The approximation is made with the assumption that the relay output consists only of the fundamental sinusoidal input. For this to hold, it is necessary that the feedback signal generated by the relay output be a pure sinusoid. Since a relatively high-order system exists (i.e., one with considerable low-pass filtering), this assumption appears valid. Since the ideal relay presents zero phase shift, the following described transfer function is defined in amplitude only:

*Thaler, G. J. and Marvin P. Pastel. Analysis and Design of Nonlinear Feedback Control Systems. Chapter 4. New York, McGraw-Hill, 1962.

Describing function

$$G_D = \left| \frac{F_{(A,\omega)}}{A} \right| \angle \phi \tag{35}$$

where

A = amplitude of input sinusoid to cause saturation

$F_{(A,\omega)}$ = amplitude of output sinusoid

ϕ = phase angle between input and output functions

For the system under study, assume a maximum input sensitivity A of 0.1 volt and an output $F_{(A,\omega)}$ of 30 volts. Then

$$G_D = 300 \angle 0^\circ \tag{36}$$

The block diagram of the servo system is now reduced to that shown in Fig. 9. It is observed that the effect of the nonlinear component G_D on the control system is to introduce a variable forward loop gain. When large errors and transients exist in the control system the forward loop gain is minimized since the input A of the describing function, Eq. (35), increases while the output F remains constant. The maximum forward loop gain occurs under steady-state operation when the control-system feedback is just sufficient to trigger the relay (flip-flop).

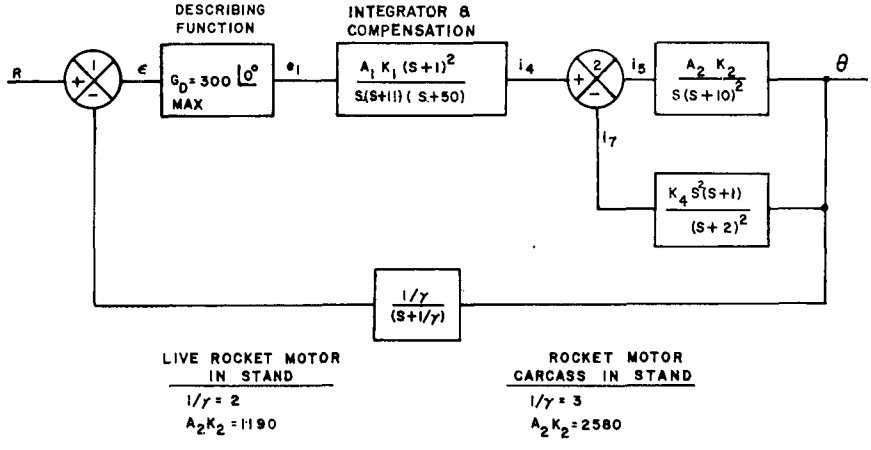

FIG. 9. Diagram Showing Further Simplification of the Compensated Control System.

ROOT LOCUS STABILITY ANALYSIS

Once the describing function has been defined it is possible to examine the servo performance by the root locus method. Since the nonlinear element is considered to introduce variable gain only, the locus of roots will not be affected and only a single overall curve is required to depict servo performance as a function of forward loop gain.

The uncompensated control system of Fig. 10 yields the root-locus plots of Figs. 11 and 12. It is evident that the uncompensated system is unstable for all values of gain. It is also evident that the addition of zeros along the negative real axis (i.e., (S + A) terms in the numerator of KGH_1) will tend to shift the root locus into the left-half plane and in general stabilize the system. Several compensating circuits are available which can be used in the forward loop to obtain these zeros. The final compensation of the control system, as indicated in Fig. 9, was determined experimentally. It is noted that the addition of the tach feedback circuit contributes two additional zeros in the open loop transfer function. This is indicated in the equivalent series element in Fig. 13.

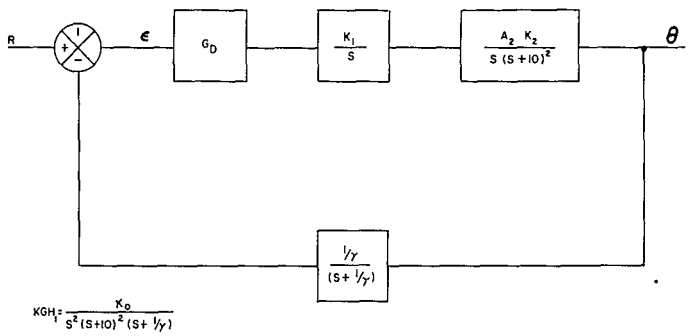

FIG. 10. Block Diagram of the Uncompensated Control System.

In the analysis of the compensated system of Fig. 9 the root-locus curve of the minor loop is plotted first and the roots of the system for a particular minor loop gain are determined. In turn, these roots are used as poles to write the overall open-loop transfer function. The root locus of the complete system is then plotted and the point of system operation is determined.

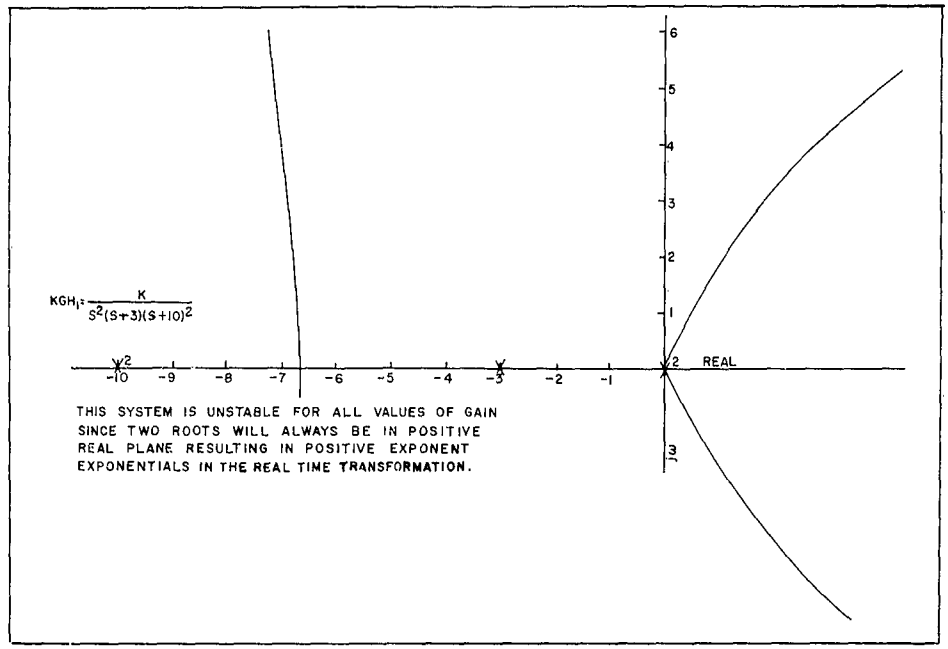

FIG. 11. Root Locus of the Uncompensated System With a Rocket Motor Carcass in the Stand.

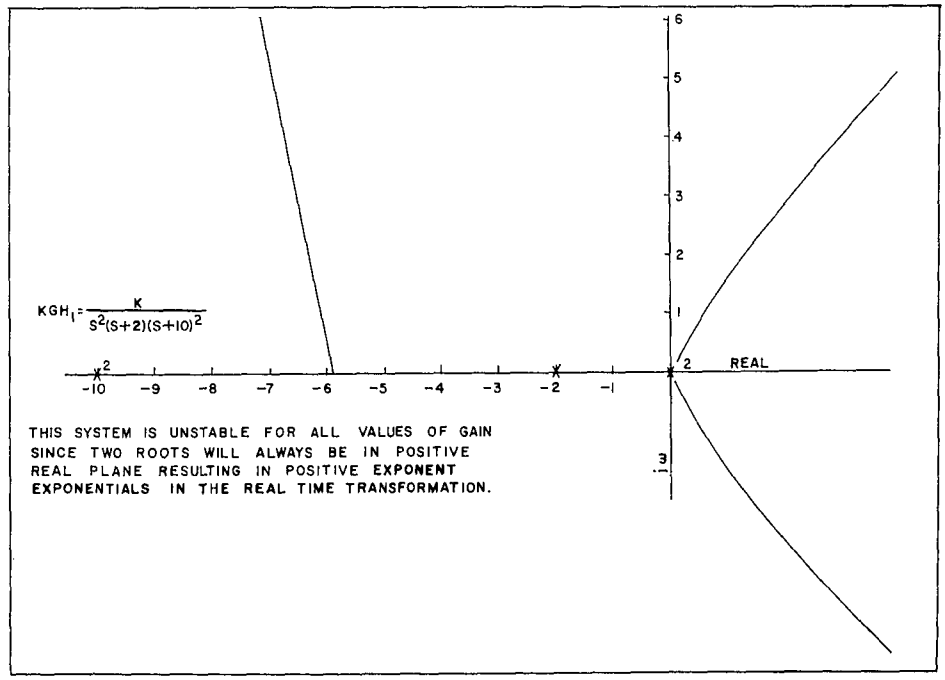

FIG. 12. Root Locus of the Uncompensated System With a Live Rocket Motor in the Stand.

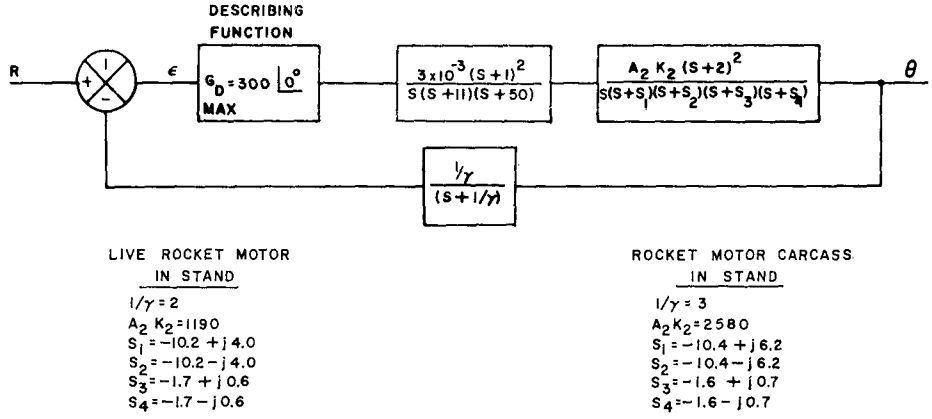

FIG. 13. Final Block Diagram of the Compensated Control System With the Equivalent Series Transfer Function Replacing the Minor Loop.

The system will be analyzed first using the system constants associated with a rocket motor carcass. The minor open-loop transfer function of Fig. 9 is given as:

$$KGH_2 = \frac{28\ S(S+1)}{(S+10)^2(S+2)^2} \tag{37}$$

$$A_2K_2K_4 = 28$$

The roots at the point of operation as determined from the locus of roots shown in Fig. 14 are as follows:

$$S_1 = -10.4 + j6.2$$

$$S_2 = -10.4 - j6.2$$

$$S_3 = -1.6 + j0.7$$

$$S_4 = -1.6 - j0.7$$

The minor-loop transfer function can now be written as follows:

$$\frac{\theta}{i_4} = \frac{A_2K_2\ (S+2)^2}{S(S+S_1)(S+S_2)(S+S_3)(S+S_4)} \tag{38}$$

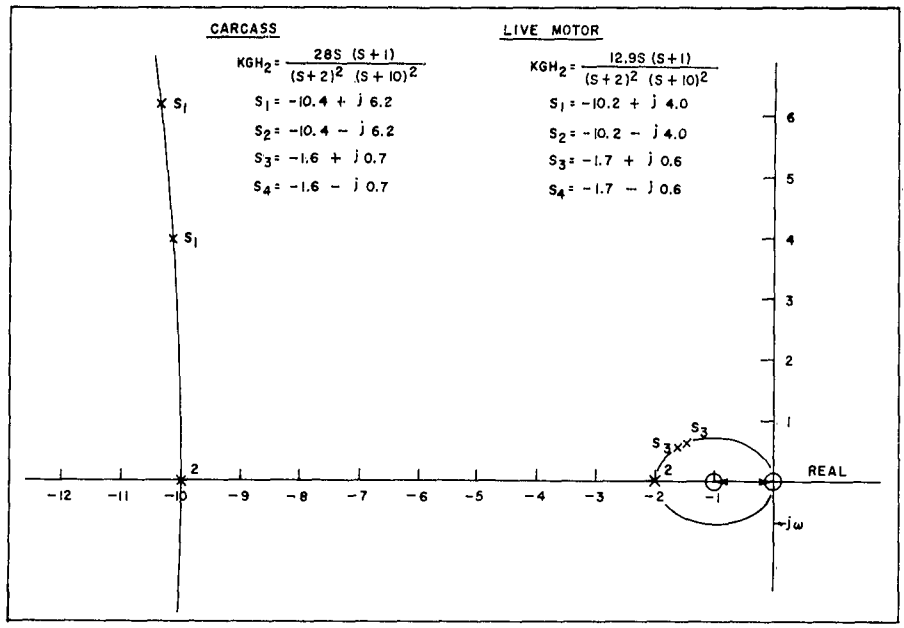

FIG. 14. Root Locus of Minor Loop.

This transfer function can now be handled as a series element in the outer loop as illustrated in Fig. 13. The outer open-loop transfer function is written:

$$KGH_1 = \frac{0.9\ A_2K_2\ (S+1)^2(S+2)^2}{\gamma\ S^2(S+11)(S+50)(S+\frac{1}{\gamma})(S+S_1)(S+S_2)(S+S_3)(S+S_4)}$$

For the motor carcass condition $A_2K_2 = 2,580$ and $\gamma = 1/3$ seconds.

$$KGH_1 = \frac{7000\ (S+1)^2(S+2)^2}{S^2(S+50)(S+3)(S+11)(S+S_1)(S+S_2)(S+S_3)(S+S_4)} \qquad (40)$$

The root-locus plot for this open-loop transfer function is shown in Fig. 15.

The same procedure is followed in plotting the overall root locus with a live rocket motor in the stand. Since the minor-loop gain is changed for this condition, a new KGH_2 must be plotted and another set of roots determined. Thus,

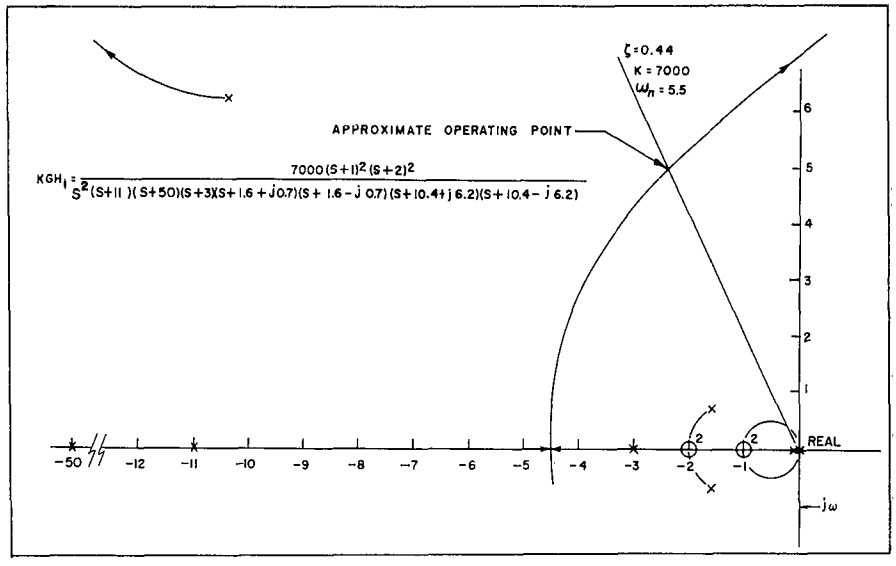

FIG. 15. Root Locus of the Compensated System With a Rocket Motor Carcass in the Stand.

$$KGH_2 = \frac{12.9\ S(S+1)}{(S+2)^2(S+10)^2} \tag{41}$$

$$A_2K_2K_4 = 12.9$$

The roots at the point of operation as determined from the locus of roots in Fig. 14 are as follows:

$$S_1 = -10.2 + j4.0$$

$$S_2 = -10.2 - j4.0$$

$$S_3 = -1.7 + j0.6$$

$$S_4 = -1.7 - j0.6$$

The minor-loop transfer function can now be written:

$$\frac{\theta}{i_4} = \frac{1190\ (S+2)^2}{S(S+S_1)(S+S_2)(S+S_3)(S+S_4)} \tag{42}$$

This transfer function is now handled as a series element in the outer loop and the following open-loop transfer function is written:

$$KGH_1 = \frac{3340\ (S+1)^2\ (S+2)^2}{S^2(S+11)(S+50)(S+2)(S+S_1)(S+S_2)(S+S_3)(S+S_4)} \qquad (43)$$

The root-locus plot for this open-loop transfer function is shown in Fig. 16. It is interesting to note that the loci of Figs. 15 and 16 are dependent only on the linear system. The effect of the variable-gain nonlinearity (describing function) is to move the root position along the locus.

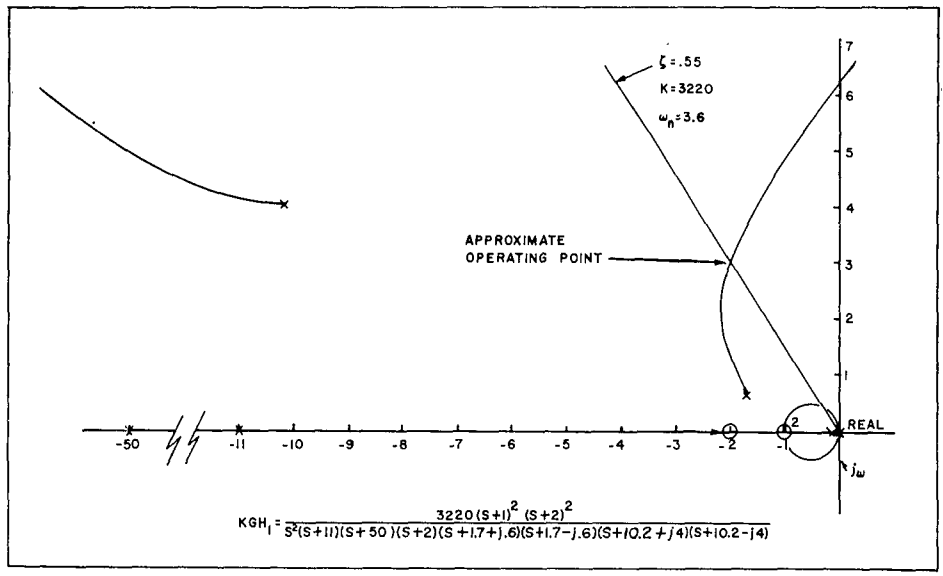

FIG. 16. Root Locus of the Compensated System With a Live Rocket Motor in the Stand.

In a relay servo system of the type under analysis, maximum gain occurs under minimum error conditions. It is seen that the roots for this condition are located at their greatest displacement from the open-loop poles. For a large initial disturbance, such as a step change in mass, the gain is low and the system will exhibit a low natural frequency. It is evident, then, that in this type of servo system the maximum gain operating point should produce a system damping ratio somewhat lower than the nominal value of 0.7. The system under study was experimentally tuned at the high-frequency end point (or in accordance with the root locus of Fig. 15). The approximate operating point indicates a damping ratio of 0.44 and an undamped natural frequency of 5.5 rad/sec.

It should be pointed out that considerable error may be present in the calculation of the maximum describing function gain. It is felt that the experimentally determined threshold sensitivity of the phase-comparator flip-flop configuration may be in error by as much as 50%. An increase in forward-loop gain of this magnitude would greatly increase the natural frequency but would tend to make the system unstable. An interesting point in favor of this type of servo system, however, is its ability to operate very near the imaginary axis while maintaining complete stability. This is best understood by visualizing the large change in gain which takes place when the system is oscillating about the zero error point. At the minimum error point the describing function gain is approximately 300. This corresponds to a phase-angle error (i.e., phase angle difference from 90° between the forcing function and displacement function) of about 1°. Under maximum error conditions, or at a 1% frequency error, a phase-angle error of about 10° is evident. This reduces the describing function gain to 30. Thus, a total forward-loop gain reduction by a factor of 10 has taken place. This tends to stabilize the system by sluggishly reducing the phase error to zero.

PERFORMANCE CHARACTERISTICS

Because of the rocket-motor malfunction that precluded completion of the second evaluation test, limited data were obtained with the system operating as a relay type with sampling. The data obtained were observed, but not recorded. The steady-state performance characteristics were observed using a rocket-motor carcass as the mass environment. The experimental results are interpolated on Fig. 17. Figures 17 and 18 also show curves of the experimental results obtained with the system operating as used in the first evaluation test; i.e., as a straight sampling type.

To obtain the curves of these figures, the control system (straight sampling type) was first operated using a live rocket motor as the mass environment. A step change in mass was approximated by closing the forward loop as the system was oscillating out of resonance with phase error. The system responded to peak overshoot in approximately 1.4 sec and settled to within 1% of the undamped natural frequency in about 3 sec. The driving-function response for this condition is plotted in Fig. 18. A steady-state oscillation about the natural frequency of 1/3 cps was observed with an 0.8% maximum deviation from the mean.

With a rocket-motor carcass mounted in the stand, the system responded to peak overshoot in approximately 1.5 sec and settled to within 1% of the undamped natural frequency in approximately 2.1 sec. A steady-state oscillation about the natural frequency of 1/2 cps was observed with a 0.5% maximum deviation from the mean. The driving-function response for this condition is shown in Fig. 17.

It is evident from the curves of Fig. 17 that the system exhibits improved transient characteristics when operated as a relay type with sampling and maintains steady-state characteristics comparable to those observed when the system was operated as a straight sampling type. The root locus plot of Fig. 16 indicates that the transient-response characteristics will be somewhat less desirable with a live rocket motor in the stand than it was with the rocket-motor carcass due to the lower gain and resonant frequency of the system at the operating point.

Techniques have been developed for theoretically approximating the limit-cycle frequency and transient response of relay servos.* The technique described in the Analysis and Design of Nonlinear Feedback Control Systems incorporates the use of the describing function and root-locus plot. An iterative process is involved and although some degree of accuracy is attainable, the analysis becomes very laborious in high-order systems. In general, for practical purposes, the techniques which have been developed for transient analysis of nonlinear servos are limited to third-order systems or lower. As a very rough approximation, however, it is possible to make the following calculation. Consider the equation given for the resonant frequency of a lightly damped second-order system:

$$\omega_r = \omega_n\sqrt{1 - \zeta^2} \tag{44}$$

In a lightly damped system the transient time from t = 0 to peak overshoot is approximately equal to one-half cycle of the resonant frequency oscillation time. Therefore, from the root locus plot in Fig. 15:

$$\omega_r = 5.5\sqrt{1-0.44^2} \tag{45}$$

From this

$$t_p = 0.7 \text{ sec}$$

From Fig. 16:

$$\omega_r = 3.6\sqrt{1-0.55^2} \quad , \text{ and} \tag{46}$$

$$t_p = 1.25 \text{ sec}$$

*Thaler, G. J. and Marvin P. Pastel. Op. cit., pp. 183-190.

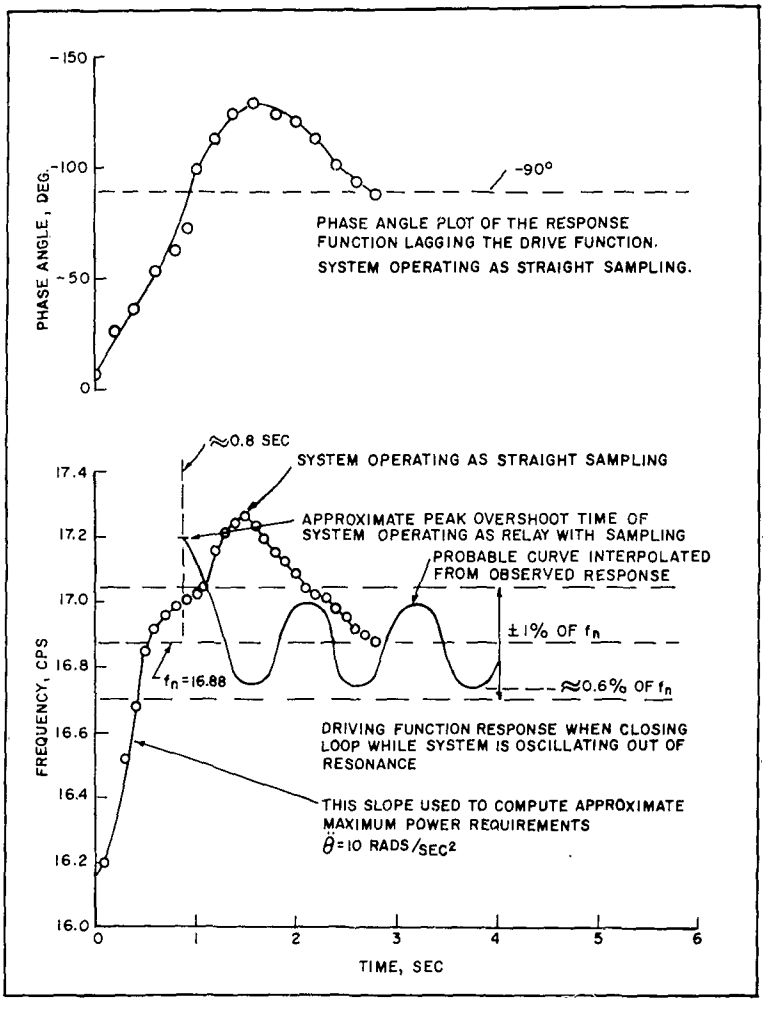

FIG. 17. Experimental System Response as a Function of Time to a Simulated Step Input (Rocket Motor Carcass).

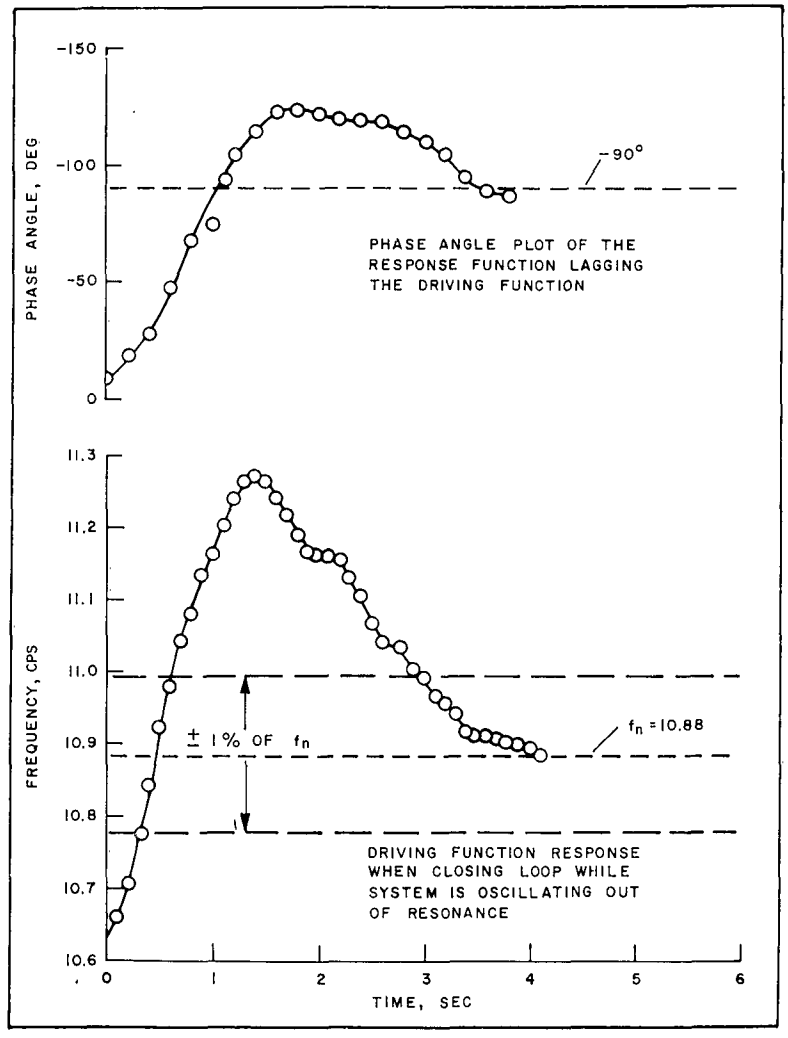

FIG. 18. Experimental System Response as a Function of Time to a Simulated Step Input (Live Rocket Motor), System Operating as a Straight Sampling Type.

A measure of agreement is evident between the value of 0.7 seconds and the experimental data. It is reasonable to assume that the value of 1.25 seconds is equally representable and that the transient response of the relay type system would also show improvement over the straight sampling type at the low frequency operating point.

In developing a high-order system with relay and other nonlinearities, theoretical calculations must be used only as a building block. That is, the theory is used to establish a first approximation from which components having a wide controllable range of values are designed or selected. In system optimization, the root-locus plots become very valuable in pointing out the compensation needed for improved performance. For instance, several possibilities for further system refinement can be listed from the root locus plots of Figs. 15 and 16. The difference between these plots can be attributed mainly to the change in minor-loop gain in traversing from one operating point to the other. It follows, therefore, that an increase in the minor-loop gain would very probably improve system performance even further. The primary restriction to this is steady-state error and instability both of which are affected by forward-loop gain. The main objective is to establish the maximum undamped natural frequency for an allowable steady-state error thus optimizing the system's transient response. Modification of the compensating circuit in the forward loop could be made to shift the root locus more into the negative plane. This would also improve the transient response.

Additional experimental data were obtained to determine the validity of the assumption that a single degree of freedom system existed.

Figure 19 shows a plot of the front and rear displacements of the stand legs into the steel springs with a rocket motor carcass in the stand; Fig. 20 plots the displacement with a live rocket motor in the stand. Although the stand was statically decoupled, it is apparent that a two-degree-of-freedom system existed consisting of two modes--pitching and translational. A look at the equations for this type of system is revealing. The equations for a completely coupled two-degree-of-freedom system (Appendix B) are as follows:

$$M(t)\ddot{Z} + (C_f+C_r)\,\dot{Z} + (\ell_r C_r - \ell_f C_f)\dot{\psi} + (K_f+K_r)Z + (\ell_r K_r - \ell_f K_f)\psi = m\ell\omega_o^2 \sin\omega_o t \qquad (47)$$

$$J(t)\ddot{\psi} + (\ell_f^2 C_f + \ell_r^2 C_r)\dot{\psi} + (\ell_r C_r - \ell_f C_f)\dot{Z} + (\ell_f^2 K_f + \ell_r^2 K_r)\psi + (\ell_r K_r - \ell_f K_f)Z = 0 \qquad (48)$$

By statically decoupling the system (i.e., by adjusting K_r and K_f so that $\ell_f K_f - \ell_r K_r = 0$), the equations are simplified to Eqs. (49) and (50). The center-of-gravity shift was found experimentally to be small so that ℓ_r and ℓ_f remain constant. Therefore,

$$M(t)\ddot{Z} + (C_f + C_r)\dot{Z} + (\ell_r C_r - \ell_f C_f)\dot{\psi} + (K_f + K_r)Z = m\ell\omega_o^2 \sin\omega_o t \qquad (49)$$

$$J(t)\ddot{\psi} + (\ell_f^2 C_f + \ell_r^2 C_r)\dot{\psi} + (\ell_r C_r - \ell_f C_f)\dot{Z} + (\ell_f^2 K_f + \ell_r^2 K_r)\psi = 0 \qquad (50)$$

This statically decoupled system is still coupled dynamically through damping, resulting in the data shown in Figs. 19 and 20. It was later determined that the thrust takeout member was also contributing a pitching moment.

The major trouble caused by the pitching mode is that at some time during burning the pitching-mode frequency is equal to the translational mode. At this point, phase errors are introduced into the translational sensors and the control loop will not function properly. Since it was not possible during design to compute the actual damping encountered, Figs. 19 and 20 represented the first concrete information obtained on damping. Despite the knowledge that the existence of a pitching mode would affect the accuracy of the data, the firing was conducted.

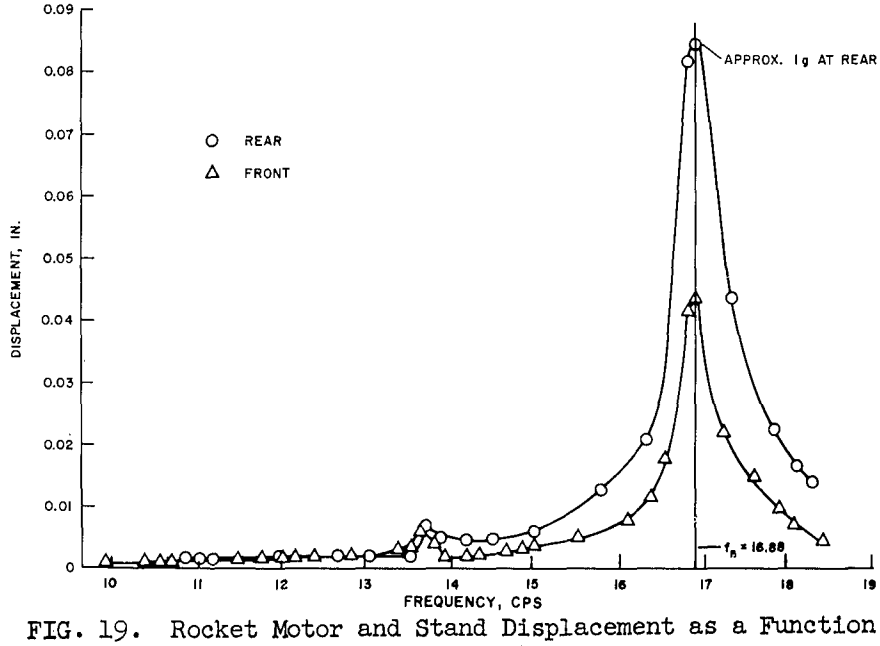

FIG. 19. Rocket Motor and Stand Displacement as a Function of Frequency (Rocket Motor Carcass).

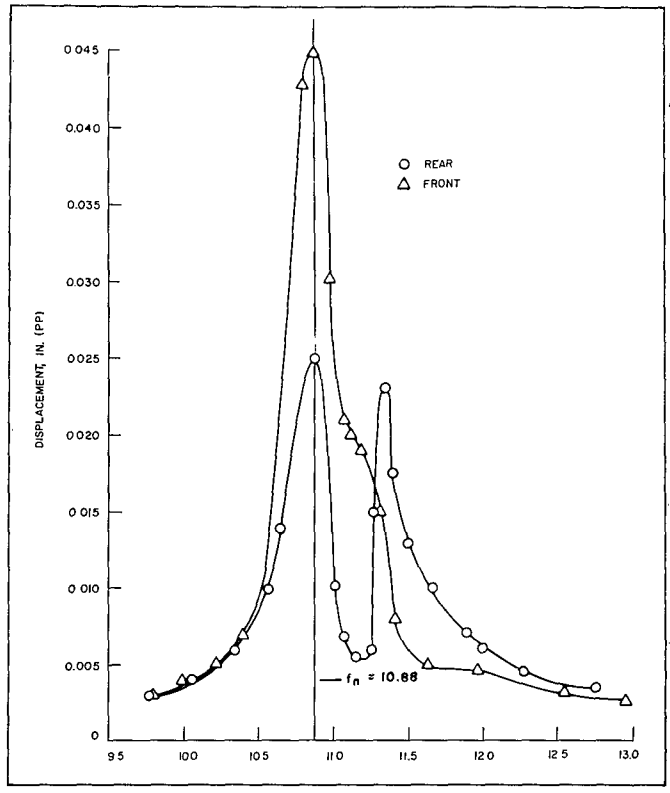

FIG. 20. Rocket Motor and Stand Displacement as a Function of Frequency (Live Rocket Motor).

LIVE MOTOR FIRING

An evaluation test of the experimental system with the NOTS-designed three-component static thrust stand was conducted with the firing of a large rocket motor on 29 June 1962. The system was operated as a straight sampling type. With the live motor mounted in the stand and the mass-measuring system in operation, a natural frequency of 10.88 cps was indicated. This reflects a corrected propellant mass (calculated mass minus the mass of the motor-stand hardware) of approximately 466 slugs or a propellant weight of 15,000 lb. At the end of burning a natural frequency of 16.88 cps was indicated--which reflects a motor-stand hardware weight of approximately 10,000 lb.

The control system remained locked-in throughout burning and the natural frequency of the spring-mass system during burning was obtained. The first full-scale demonstration of the feasibility of this technique for determining mass during burning is shown in a plot of mass versus burning time derived from the natural frequency data (Fig. 21).

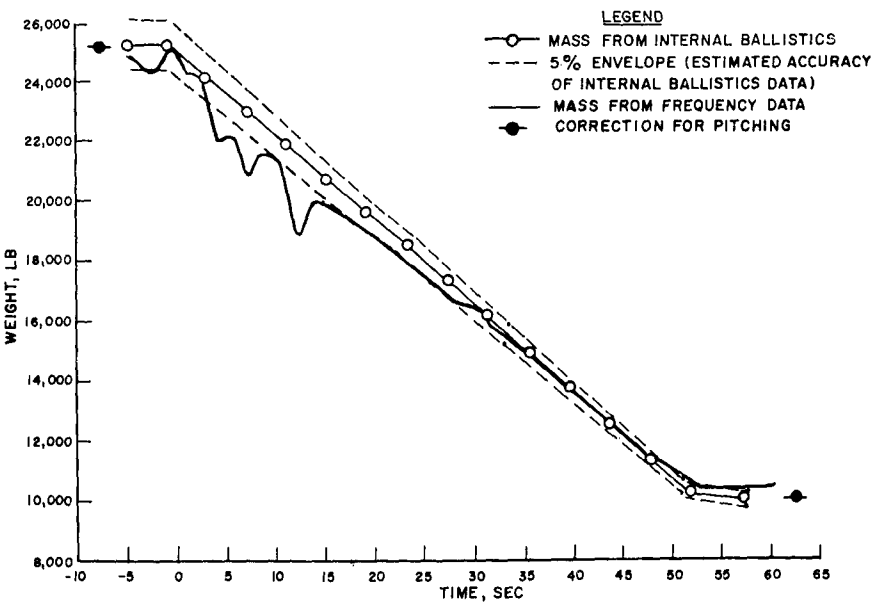

FIG. 21. Vibrating Mass as a Function of Burning Time.

It is evident from Fig. 21 that, except for the period from 5 to 15 sec during burning, the calculation of mass using natural-frequency information is generally within 2% of the mass as derived from internal ballistics or pressure information. The graph was plotted by smoothing or averaging the data to obtain a point for each second of operation.

Several anomalies are apparent in the 5- to 15-sec period of burning. Analysis of the data of the front and rear displacement sensors indicates that the pitching motion is predominately active during this state of operation since the natural frequency of the pitching mode is equal to that of the translational mode during this period. It is apparent that the control system is attempting to lock-on the pitching mode and is thus switching between the pitching and translational motions. The natural frequency of the pitching mode and the natural frequency of the translational mode increase with a decrease in mass but the pitching mode frequency increases at a much lower rate. Therefore, after 15 sec of burning, the natural frequency of the pitching mode is sufficiently separated from the desired translational natural frequency so that its interference with the control system is minimized. Mass calculations from this point to the end of burning, using frequency data, are generally within 2% of the mass plotted from the internal ballistics data.

The pitching motion contributes additional error since the magnitudes of the displacement sensors, which are located over the front and rear springs, are not equal. Since the waveform representing system response is obtained by summing the sinusoidal outputs of the sensors, it has a phase relationship dependent upon displacement magnitude. The extent to which this adds to frequency error is not known since true-system response is not readily available from existing data; however, in a spring-mass system with a very small damping ratio (approximately 0.1%), a relatively large phase error, say 10°, would result in an approximate 1% error in the natural frequency and an approximate 2% error in mass calculation.

Another factor associated with the pitching motion which contributes directly to error in calculations of mass is the assumption that

$$M = \frac{K_f + K_r}{\omega_n^2} \tag{51}$$

This equation describes a spring-mass system with a single degree of freedom. To derive the approximate equation including the pitching mode, consider a spring-mass system with little damping, wherein:

$$\frac{PE}{KE} = 1$$

$$\frac{\frac{1}{2}(K_f+K_r)\ Z_m^2 + \frac{1}{2}(\ell_f^2 K_f + \ell_r^2 K_r)\ \theta_m^2}{\frac{1}{2}\ M(\omega_n Z_m)^2 + \frac{1}{2}\ J(\omega_n \theta_m)^2} = 1$$

Solving for mass:

$$M = \frac{(K_f + K_r)\ Z_m^2 + (\ell_f^2 K_f + \ell_r^2 K_r)\ \theta_m^2}{\omega_n^2\ Z_m^2} - \frac{J\theta_m^2}{Z_m^2} \qquad (52)$$

where

PE = maximum potential energy, lb-ft

KE = maximum kinetic energy, lb-ft

J = inertia, lb-ft-sec^2

ℓ_f = distance from c.g. to forward support, ft

ℓ_r = distance from c.g. to rear support, ft

K_f = front spring constant, lb/ft

K_r = rear spring constant, lb/ft

C_f = front damping, $\frac{\text{lb-sec}}{\text{ft}}$

C_r = rear damping, $\frac{\text{lb-sec}}{\text{ft}}$

Z_m = maximum vertical displacement, ft

ω_n = natural frequency vertical plane, rad/sec

θ_m = maximum pitching angle, rad

A rough calculation using quick-look analog data for obtaining θ_m and estimating a value for J has shown that an error of 2% in mass determination is probable if the simplified mass equation is used (see Fig. 21 for correction of the two end points).

Another possible source of error in the determination of mass is spring nonlinearity. A dynamic spring constant can be derived as follows:

$$\omega_{n_1}^2 = \sqrt{\frac{K}{M_L}} \qquad \text{and} \qquad \omega_{n_2}^2 = \sqrt{\frac{K}{M_B}}$$

where

M_L = mass of live motor

M_B = mass of motor carcass

Rearranging, the equation becomes

$$M_L = \frac{K}{\omega_{n_1}^2} \qquad \text{and} \qquad M_B = \frac{K}{\omega_{n_2}^2}$$

and combining terms, gives

$$M_L - M_B = \frac{K}{\omega_{n_1}^2} - \frac{K}{\omega_{n_2}^2}$$

Again rearranging, the equation becomes

$$\Delta M = K\left(\frac{1}{\omega_{n_1}^2} - \frac{1}{\omega_{n_2}^2}\right)$$

and finally,

$$K_{(dy)} = \left(\frac{\Delta M}{\omega_{n_1}^2 - \omega_{n_2}^2}\right) \tag{53}$$

Using the end point frequencies and the change in mass obtained by weighing the rocket motor before and after burning, a dynamic spring constant of 3.72×10^6 lb/ft was obtained. This figure is within approxi-

mately 4.5% of the average calculated spring constant of 3.56×10^6 lb/ft obtained using static deflections and known weights in the mass calculations shown in Fig. 21. Although the pitching mode has been neglected in calculating for $K_{(dy)}$, this magnitude of difference suggests that a a measure of nonlinearity may exist.

Analysis of the data from this firing in correlation with the analog computer study (Appendix A) indicates that the discrepancy in the calculation of mass from actual frequency as compared with internal ballistics data can be attributed to the existence of the pitching mode and to the momentary loss of vertical displacement.

It is estimated that using the simplified equation, mass $= \frac{K}{\omega_n^2}$ (which neglects the pitching mode) contributed an error of approximately 2% in the computation of mass. It should be noted, however, that information obtained in the simulation study indicated that the pitching mode error as well as the error in the indicated natural frequency may be due to an additional form of damping or structural phenomena.

Experimental tests were conducted to determine what types of damping existed and if undesirable structural oscillations were present. It was found that structural as well as viscous damping existed and that pitching was being introduced by coupling through damping and by the moments generated by the structural oscillation of the thrust take-out member.

Although structural damping adds to the nonlinearities of the system, it is not particularly undesirable in system operation since, in the translational mode, the undamped natural frequency is independent of such damping. It was observed that the natural frequency of the thrust take-out member was approximately 15 cps. With this relatively low natural frequency, the member was being excited through the oscillations in the translational mode. A solution to this problem might be to stiffen the thrust take-out member (which can be accomplished quite easily) to raise its natural frequency and thus reduce the energy transmitted from the translational mode. The pitching motion further introduced error in the phase relationship of the displacement waveform. This spurious error in phase relationship was the result of sensing the unequal translational motion of the rocket motor at the front and rear supports and was reflected in the control system as true freqency error. The frequency error from this source (generally spasmodic) is predominately active during the first 15 sec of burning. It was observed that the pitching motion was most active during this period when the natural frequency of the pitching mode was equal to and traversed by the continually increasing natural frequency of the spring-mass system.

Momentary loss of vertical displacement resulting both from excessive phase error and contributions from external disturbances caused an overexcitation of the control system. In this state, large magnitudes of oscillation are introduced and the system approaches instability. These oscillations are apparent in the 5- to 15-sec period of burning.

CONCLUSIONS AND RECOMMENDATIONS

The theoretical analysis presented in this report gives a reasonable prediction of the mass measurement system performance. As well as providing component design criteria, the root-locus method becomes a convenient tool for field optimization of the system. The nature of the root-locus method is such that the time constant of each component is easily obtained and its affect on the system can be determined. The affect of various types of compensating circuits (i.e., lead, lag, lead-lag, or lag-lead) on the root locus, and hence on the system, can also be conveniently determined.

The assumption that the spring-mass nonlinear transfer function can be replaced with that of a simple RC lag network is not theoretically justified. It is clear, however, from the analog studies that a lag does exist in the feedback loop due to sudden changes in mass. It is also clear that the time response of the lag changes between the two end points of operation. This is probably due to a change in system damping between these operating points. A detailed analysis of this lag is described in NAVWEPS Report 7741 (see Bibliography). This report describes an electrical analog of the spring-mass system which is designed and constructed. The breadboard model is laboratory tested to determine the lag characteristics.

The experimental system, through the successful firing of a large rocket motor, has demonstrated the feasibility of this technique for determining the mass of large rocket motors during burning.

The steady-state performance characteristics indicate that the system (straight sampling type) is capable of maintaining a translational oscillation within 1% of the undamped natural frequency of the spring-mass system. A 1% frequency error in a single degree of freedom system will correspond to an approximate 2% error in mass measurement. Since the present methods of mass determination are considered to have an accuracy of 5%, it is obvious that the new technique will improve accuracies significantly. The main limitation of the experimental system is its inability to respond rapidly to sudden changes in mass burning rates. It is estimated that sudden mass changes in the order of 1% of the total vibrating mass could be detected. Detailed information on the mass burning rates during a period of irregular burning cannot be obtained because of the smoothing or integrating characteristic of the control system.

It is pointed out that this experimental system was developed primarily to demonstrate the feasibility of this technique of mass measurement. Considerable improvements can be incorporated into an operational system to improve steady-state and transient characteristics. Several of these improvements are discussed in the following paragraphs.

OPERATIONAL SYSTEM

As noted above, the design of an operational control system involves two prime considerations: minimization of steady-state error and maximization of frequency (transient) response. The experience gained in the successful operation of the experimental system has provided considerable insight in the selection of components to adequately meet these two major objectives. Following are several suggested improvements for each of the major experimental system components.

Force Generator

The force generator used in the experimental system was a mechanical device with rotating parts (Fig. 5). Although the device generated a fairly smooth sinusoidal waveform some backlash did exist. This backlash appeared minimal and was not considered in the theoretical anaylsis; however, the existence of backlash is certainly undesirable. The force generator was driven with a DC motor which in turn was controlled by a magnetic amplifier. This relatively long power train results in excessive response lags and ultimately limits the frequency response of the closed-loop system. As an improvement for this portion of the system it is recommended that an electrodynamic shaker be employed. Electrodynamic shakers that will fulfill frequency and force output requirements are commercially available. In addition to the advantage of generating a smooth undistorted waveform, the main improvement the electrodynamic shaker provides is a large reduction in response time. It is estimated that the response times associated with this portion of the experimental system could be reduced by a factor of 10 with the selection of a suitable electrodynamic shaker. These shakers are available with both velocity and acceleration feedback so that a closed-loop system similar to that of the experimental system could be used.

Phase Comparator

The phase comparator used in the experimental system was a sampling device in that the phase error was determined at each zero crossover of the displacement wave. It is apparent that an improvement in system operation could be realized if a phase comparator were available for a continuous comparison of the phases of two sinusoidal waveforms. The complication is in the design of a phase comparator capable of comparing the phase relationship of two waveforms, one of which exhibits a variable amplitude. Some methods of low frequency phase detection are described in a paper by T. F. Bogart, Jr.*

*Technical paper dated January 1963 written to fulfill thesis requirement for a Masters Degree at the University of California, Los Angeles.

Another method of improving this portion of the control system would be to use a sampling phase comparator as was used in the experimental system and increase the sampling rate. Although the following methods have not been investigated in detail, this effect might be accomplished through the use of frequency multipliers of electronic type or, in the case of the sine-cosine potentiometer, through a simple gearing arrangement.

Spring-Mass Dynamics

Although this area has been touched only lightly in this report it remains a very important element in the successful use of this technique of mass measurement. The static thrust stand must be designed to meet special requirements. The stand must be adjusted in the field to eliminate entirely if possible, or to at least minimize, pitching. This would enable the use of single degree of freedom theory and much simpler operation. NAVWEPS Report 8353* describes the design criteria for construction of thrust stands to be used with this technique of mass measurement.

1% System

It is felt that modification of the control system described in this report to incorporate the use of an electrodynamic shaker and by careful thrust-stand design, a system can be developed which will provide for the determination of mass to an accuracy of better than 1% and will enable the extraction of data on instantaneous burning rates during periods of irregular burning.

*U. S. Naval Ordnance Test Station. Design Criteria for Large Accurate Solid-Propellant Static-Thrust Stands, by D. P. Ankeney and C. E. Woods. China Lake, Calif., NOTS, June 1963. (NAVWEPS Report 8353, NOTS TP 3240).

Appendix A

ANALOG SIMULATION

Data analysis of the first evaluation firing using the mass measuring system pointed out some apparent anomalies in the data and in the system's overall performance. In order to better define system behavior and to predict minor in-house modifications which could be made to the experimental system before conducting the second evaluation firing* an analog computer simulation of the complete system was made. In addition, an investigation to determine system performance under jetavator reaction was conducted.

ANALOG SETUP

The differential equations describing the spring-mass-force system were written in two degrees of freedom (Appendix B) taking the vertical motion of the c.g. of the rocket motor and the pitching motion of the rocket motor about its c.g. into consideration. The equations were extended to include both front and rear vertical-motion sensors (potentiometers). To simulate the two-degree of freedom experimental system, the signals from the sensors were summed to provide one composite signal representing the vertical displacement of the rocket motor. A schematic of the analog simulation is presented in Appendix B.

In setting up the analog computer study it was felt that considerable valuable information (in addition to that defining general system characteristics) would be obtained if the experimental system were very accurately simulated. For instance, the same improved system performance produced in the analog simulation by small changes in electrical characteristics and minor hardware modifications could also be expected from the experimental system by making the same component changes.

The procedure used in attempting to set up the analog computer to simulate the experimental system accurately was to adjust the basic (experimental or calculated) values of various coefficients in the differential equations that were known or believed to change during burning

*The second firing was not conducted because of a rocket-motor malfunction which resulted in partial destruction of the drive motor and shaker.

and then try to retrace the vertical displacement-curve data shown in Figs. 19 and 20. To obtain data points for the curves, the system was operated open loop and the front and rear rocket-motor displacement was observed as the oscillation frequency was varied. The displacement curves of the final analog setup are shown in Figs. 22 and 23. Figures 19 and 22 are curves for a rocket-motor carcass mounted in the stand and Figs. 20 and 23 are curves for a live rocket motor mounted in the stand. In order to reproduce the curves plotted in Figs. 19 and 20 for the analog simulation, it was necessary to use time-varying functions for rocket-motor inertia, system damping, and all terms associated with a shift in rocket-motor c.g.

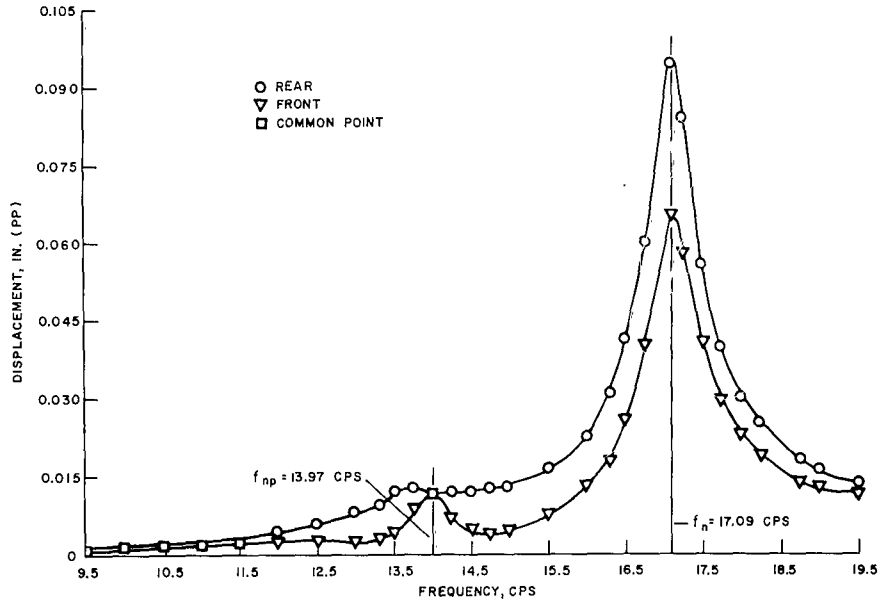

FIG. 22. Rocket Motor and Stand Displacement as a Function of Frequency (Rocket Motor Carcass), Analog Simulation.

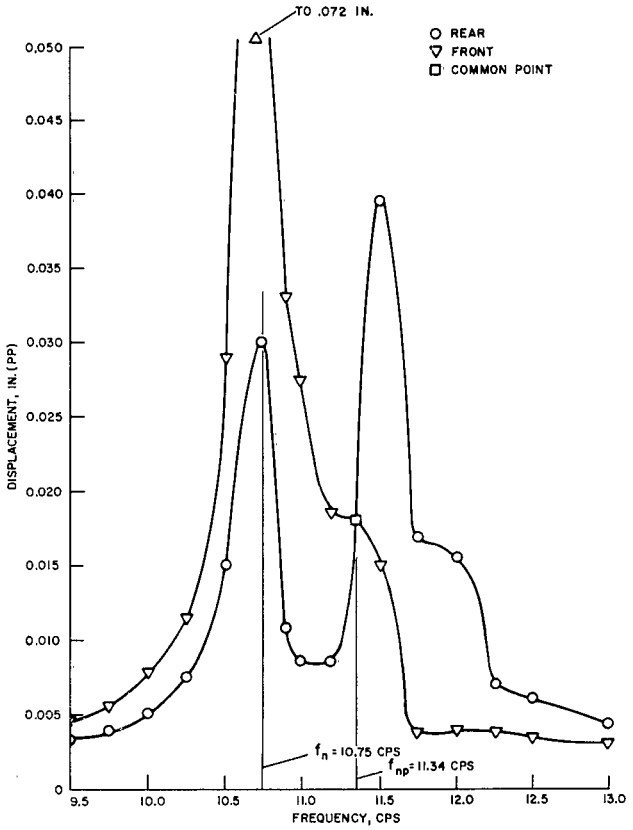

FIG. 23. Rocket Motor and Stand Displacement as a Function of Frequency (Live Rocket Motor) Analog Simulation.

The controlled functions were made to vary linearly with time from rocket-motor ignition to burnout. Curves of each function versus time appear in Appendix B. Although the displacement curves are only fairly comparable to those of the experimental system, they represent the best simulation obtainable with the present differential equations. Additional terms would be required to improve the accuracy of simulation. Structural damping, which is amplitude dependent, has been suggested as a highly probable required term--structural damping was detected in later experimental tests.

The actual differential equations solved include viscous damping only. In the final analog setup it was necessary to double the system damping from ignition to burnout. It was further necessary to reverse the distribution of the system damping between front and rear so that the damping in the rear exceeded that in the front. This was necessary

in order to reproduce the pitching evident in the experimental data. It has since been determined that the thrust take-out member was also contributing to the pitching motion.

Since the differential equations solved include time-varying coefficients, they are considered nonlinear and their degree of similarity to the experimental system, as compared by vertical displacement curves, is difficult to ascertain. It was felt however, that the major characteristics of the displacement curves were reproduced and that reasonable similarity existed.

To further compare the analog simulation and the experimental system, all of the components associated with the experimental system were simulated and tested. Response curves were obtained by monitoring the frequency of the driving function (motor speed $\dot{\theta}$) and closing the control loop while the system was oscillating out of resonance. The resulting curve indicates the system response to a step input in phase error (an approximated step change in mass). Phase error is defined as the phase difference in degrees between the forcing function and the rocket-motor-stand response function minus 90°, or:

$$\theta_e = \theta_f - \theta_r - 90^\circ$$

where θ_e is the instantaneous phase error, θ_f is the phase angle of the forcing function with respect to some reference, and θ_r is the phase angle of the rocket-motor-stand response function with respect to the same reference. The (-90°) is required since θ_f is leading θ_r by 90° at the natural frequency. The analog simulation response curves for the step input in phase error with a rocket-motor carcass and with a live rocket motor mounted in the stand are shown in Figs. 24 and 25. Figures 17 and 18 are curves from the same test conducted experimentally with the prototype system. The forward-loop gain, the feedback-loop gain, and the compensating networks of the control system were adjusted in an effort to improve the similarity between the two sets of curves. Figures 24 and 25 represent the best simulation attainable using constant control system characteristics; i.e., closed-loop gain and compensating networks.

It was noted that much better similarity could be obtained (when either the rocket-motor carcass or the live rocket motor was mounted in the stand) if the control system characteristics were adjusted under each condition. This adjustment, however, cannot presently be made in the field, and it was decided to continue the simulation study using the analog setup indicated above rather than to attempt to incorporate time-varying functions in the control system.

Considerable difference is apparent between the two sets of response curves. The degree of dissimilarity between the analog setup and the experimental system is such that the significance of the analog study will be limited to applications of a general nature.

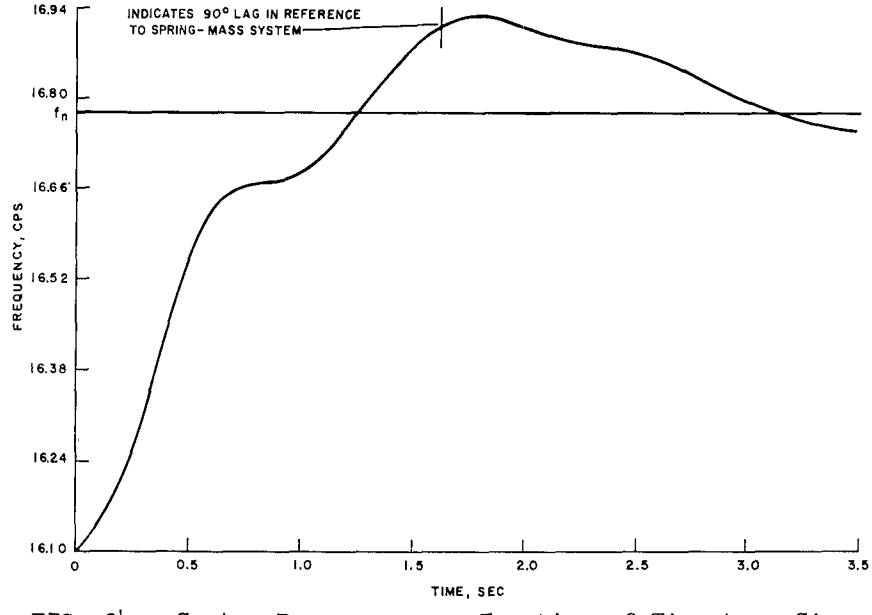

FIG. 24. System Response as a Function of Time to a Simulated Step Input (Rocket Motor Carcass), Analog Simulation.

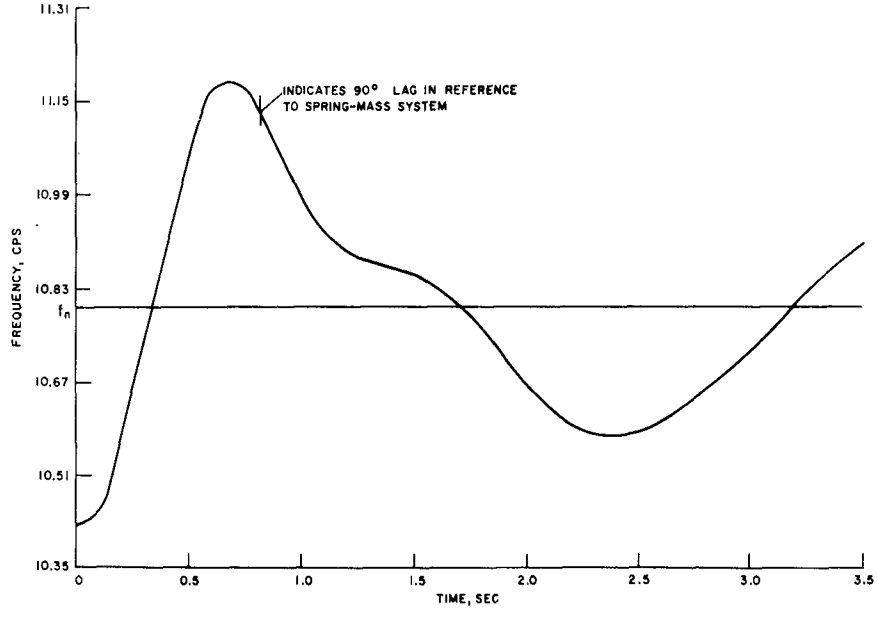

FIG. 25. System Response as a Function of Time to a Simulated Step Input (Live Rocket Motor), Analog Simulation.

COMPUTATION OF MASS

The curve of Fig. 26 is mass versus time and represents the simulated linearly changing mass. The curves of Fig. 27 are mass versus time and were obtained under closed-loop operation by computing mass from continuous knowledge of the driving-function frequency and the spring constant of the spring-mass system.

It is noted that very little difference exists between the computed curves of mass versus time with and without the pitching mode terms. That is, the computed curves of mass versus time obtained when simulating a two-degree-of-freedom spring-mass system are essentially retraced when the spring-mass system is simulated in one degree of freedom. The one-degree-of-freedom simulation was accomplished by eliminating all terms in Eqs. (49) and (50) associated with the pitching angle ψ. The resulting equation is

$$M(t)\ddot{Z} + (C_f + C_r)(t)\dot{Z} + (K_f + K_r)Z = m\ell\omega_o^2 \sin\omega_o t$$

An approximate 2% error in the mass computation due to rocket motor pitching was expected since this was the error estimated in the live motor test. This error is not apparent in the analog simulation. An appreciable amount of pitching was evident in the analog setup which tends to indicate that pitching does not contribute greatly to frequency error.

It should also be pointed out that it was not possible to excite the pitching mode when simulating a statically decoupled system. That is, when setting the term $(l_f K_f - \ell_r K_r) = 0$. This tends to indicate that damping other than viscous is present or perhaps that coupling is existent through a structural difficiency or through the shift in c.g. It was necessary to introduce a relatively large coupling term $(\ell_f K_f - \ell_r K_r)$ in order to cause pitching and enable the retracing of the displacement curves of Figs. 22 and 23. The overall accuracy in analog mass computation is improved over the indicated results of the experimental system in the evaluation firing. The error in mass computation is approximately 2% at ignition and decays to essentially zero by the end of burning.

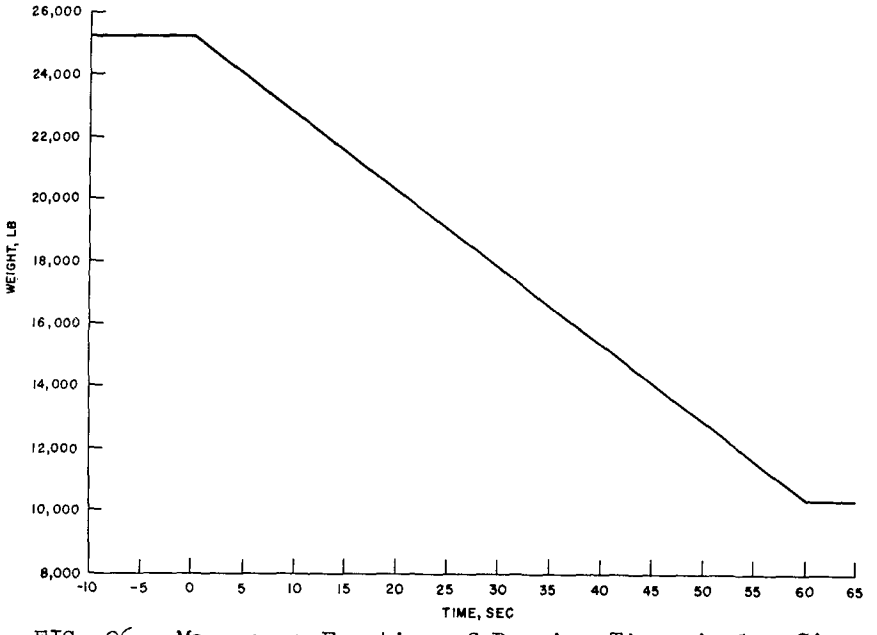

FIG. 26. Mass as a Function of Burning Time, Analog Simulation.

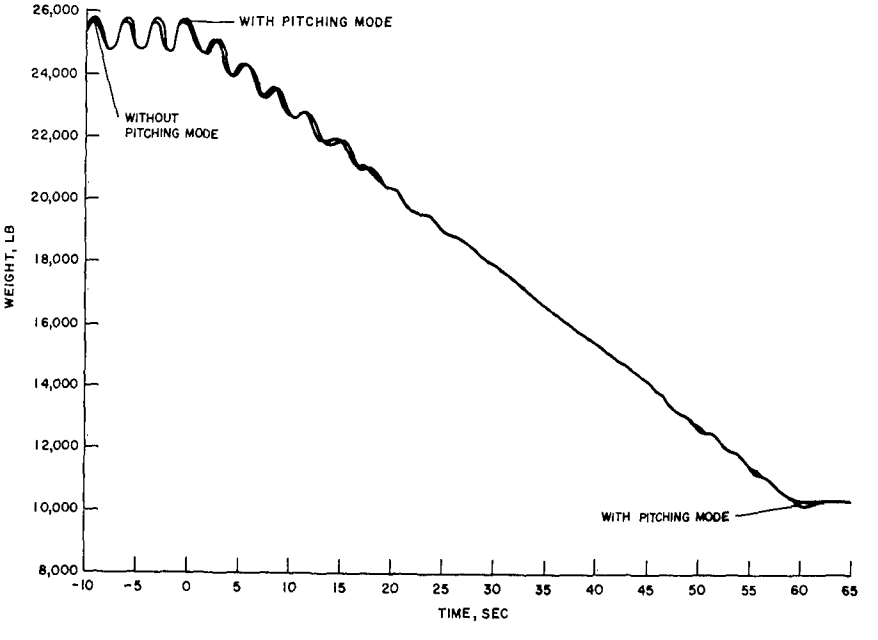

FIG. 27. Vibrating Mass as a Function of Burning Time Computed From Frequency Data, Analog Simulation.

JETAVATOR REACTION

The curves of Figs. 28 and 29 are computed mass versus time with the system being subjected to jetavator reaction of various frequencies and waveforms (Appendix B). It was found that the system as simulated was essentially unaffected (actually performance was improved) by a sinusoidal jetavator reaction frequency of 1 or 2 cps. The system became unstable as the jetavator reaction frequency approached 10 cps (sinusoidal). In each case where instability was observed, it was noted that the control loop remained unaffected and that instability took place through the progressive buildup of the vertical displacement. The system again became unstable with the application of a square wave jetavator reaction of 1-cps frequency. The system was essentially unaffected, however, when subjected to a triangular waveform with a frequency of 2 cps.

ROCKET-MOTOR LAG

From data obtained with the experimental system, it is apparent that a lag relative to changes in driving-function frequency exists in the spring-mass system. It was not known if this lagging effect would be sufficient to hinder closed-loop performance under conditions of normal or irregular propellant burning. An investigation was conducted on the analog system to better define the rocket-motor lag characteristics. The investigation consisted of effecting step changes in mass while holding the oscillation frequency of the driving function constant and observing the phase angle between the spring-mass system and the driving function. The curves in Fig. 30 show phase angle versus time for the two conditions; i.e., live and carcass rocket motors mounted in the stand. Comparison of the response curves of Figs. 24 and 25 with those of Fig. 30 shows that the response times are approximately the same in each case. While this indicates that the rocket-motor lag in a spring-mass system might very well affect overall system performance, it is noted that the simulated system did perform satisfactorily with the lag.

Although the experimental system is only generally simulated and the rocket-motor lag curves do not necessarily reflect field conditions, it is reasonable to assume that this lag does not seriously affect the performance of the present experimental system. However, if a degree of accuracy better than the presently feasible 2% is to be attained, additional investigation in this area may be necessary.

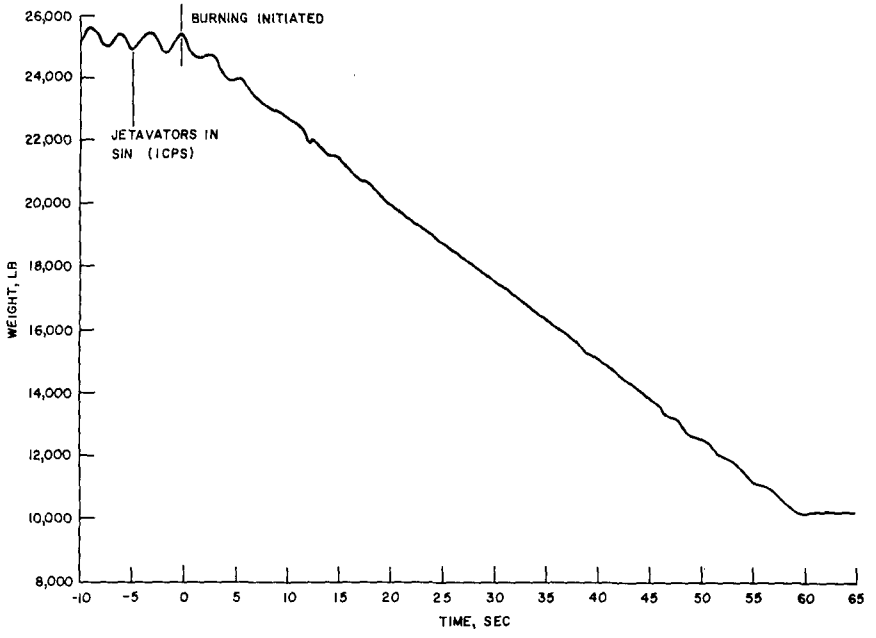

FIG. 28. Vibrating Mass as a Function of Burning Time With Jetavator Reaction, Analog Simulation.

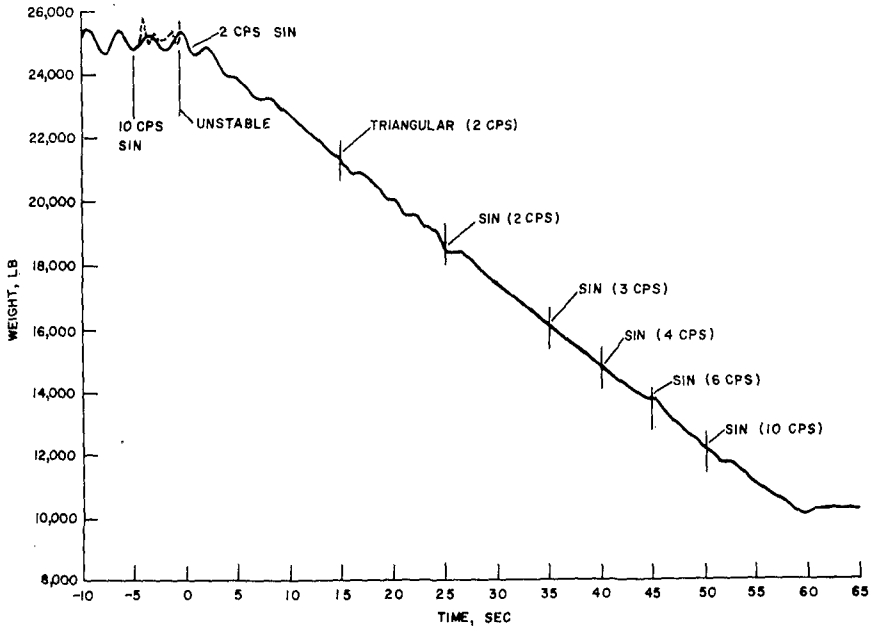

FIG. 29. Vibrating Mass as a Function of Burning Time With Jetavator Reaction, Analog Simulation.

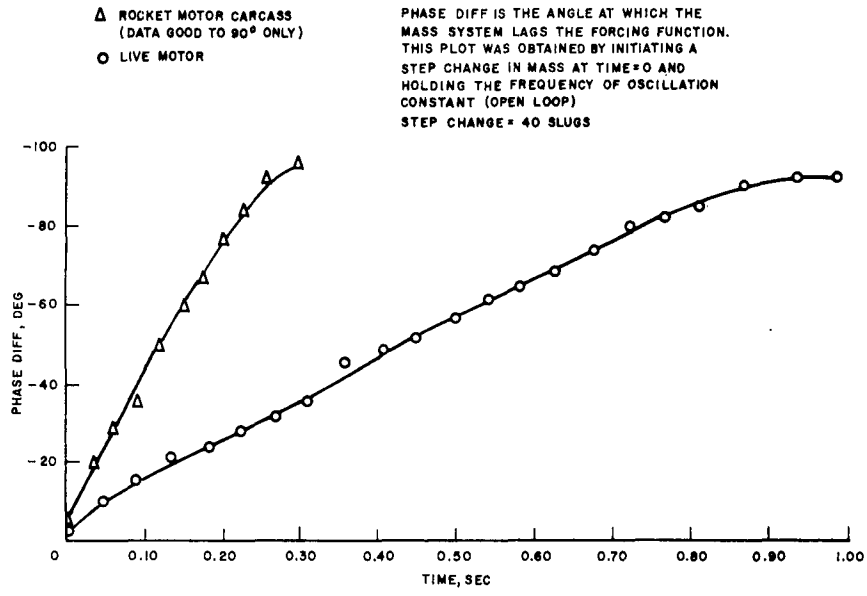

FIG. 30. Phase Angle Response of Spring-Mass System as a Function of Time, Analog Simulation.

SUMMARY

Analog computer simulation of the experimental mass measurement system was undertaken with the idea that the system could be accurately simulated and that reproduction of experimental data could be made. Detailed changes could then be made on the analog setup to study and improve system performance and, by making the appropriate changes on the experimental system, the same results could be expected.

The effective similarity between the final analog setup and the experimental system was found, however, to be questionable since only part of the data obtained with the experimental system could be reproduced in the simulation. The data reproduced are of vertical displacement versus frequency for the two conditions of a rocket-motor carcass and a live rocket motor mounted in the thrust stand. In order to obtain correlation with experimental data it was necessary to vary, linearly with time during burning, several of the coefficients of the differential equations solved. The extent to which some of these coefficients had to be varied does not appear to be practical. The conclusion is, then, that the analog setup must be considered in general terms only and that it cannot be used for detailed design studies. Since the analog setup is of the same type

of system as the experimental system (i.e., velocity-controlled, phase-sensitive) with identical type components, it is reasonable to speculate that the general system characteristics are also similar.

It should be noted that several tests conducted with the analog setup have indicated that damping is a critical factor in depicting the similarity between the analog setup and the experimental system. These tests support a previous theory that structural (amplitude-dependent) as well as viscous (velocity-sensitive) damping is existent in the experimental system. It is reasonable to assume that improved correlation could be obtained in a future study by using additional damping terms. Appropriate terms would also be required to simulate the pitching moment contributed by the thrust take-out member.

The following conclusions are based on the preceding discussion and are applied to the experimental system in terms of gross information only.

The vertical frequency characteristic of the closed-loop system (analog setup) to a linearly changing mass is one of controlled symmetrical oscillation about the mean or natural frequency. The computer setup did not produce excessive oscillation during the 5- to 15-sec period of burning as did the experimental system. This is attributed to the need for additional terms in the differential equations to cause the excessive pitching apparent in the evaluation test during this period of burning.

A rocket-motor lag to a step change in mass was apparent in the spring-mass system. The effect of such a lag on the system's performance is small, however, and should not prevent mass determination to an accuracy of 2%.

Jetavator reaction frequencies of 2 cps sinusoidal and triangular did not adversely affect system performance. The system was unstable, however, when subjected to a jetavator reaction sinusoidal frequency of 10 cps and a square wave frequency of 1 cps.

The limited computer time available did not permit an investigation of system component characteristics in relation to their affect on system performance nor an investigation of system performance when operated as a relay-sampling system (addition of relay in forward loop). Detailed information of such tests would not be direcly applicable to the experimental system since the analog setup did not exactly simulate the experimental system.

Appendix B

DERIVATION OF EQUATIONS FOR ANALOG SIMULATION AND ANALOG SCHEMATIC DIAGRAM*

SPRING-MASS SYSTEM EQUATIONS

$F_1 = 10,000 \sin \omega_{1t}$ $\quad F_o = m_o \ell_o \omega_o^2 \sin \omega_{ot}$

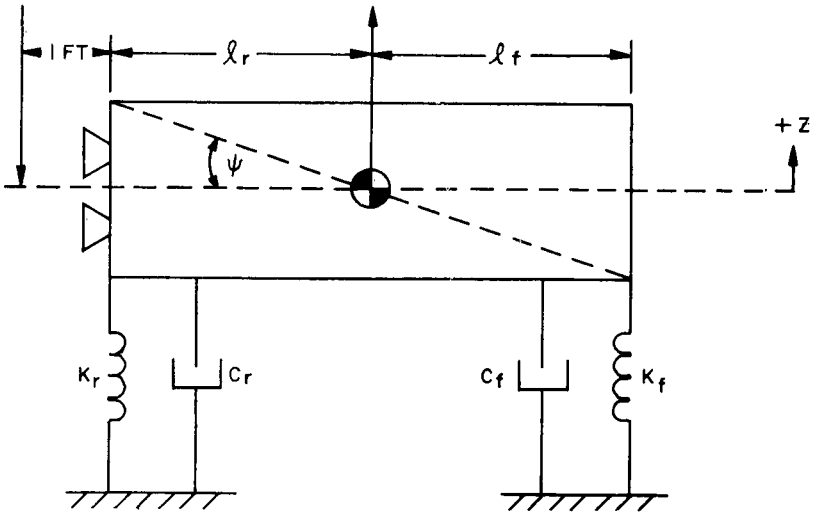

Rocket Motor Mounted in Stand
Assume two degrees of freedom
a. Vertical motion of c. g.
b. Pitching motion about c. g.

F_o = Force generated by mechanical shaker
F_1 = Force generated by jetavator

From F = ma

$$M\ddot{Z} = [\, m\ell\omega_o^2 \sin\omega_o t - (K_f + K_r)\, Z - (C_f + C_r)\,\dot{Z} - (\ell_r K_r - \ell_f K_f)\,\psi - (\ell_r C_r - \ell_f C_f)\,\dot{\psi} - 10,000 \sin \omega_1 t] \qquad (54)$$

From T = Jα

$$J\ddot{\psi} = [\, -(\ell_f^2 K_f + \ell_r^2 K_r)\,\psi - (\ell_f^2 C_f + \ell_r^2 C_r)\,\dot{\psi} - (\ell_r K_r - \ell_f K_f)\, Z - (\ell_r C_r - \ell_f C_f)\,\dot{Z} - (\ell_r + 1)\, 10,000 \sin \omega_1 t\,] \qquad (55)$$

*For symbols and variable coefficients used in this appendix, see pages 57 and 59; the analog schematic diagram appears on page 60.

MECHANICAL OSCILLATOR EQUATION*

Derivation of the equation of torque reflected into drive motor mounted on inertial axis.

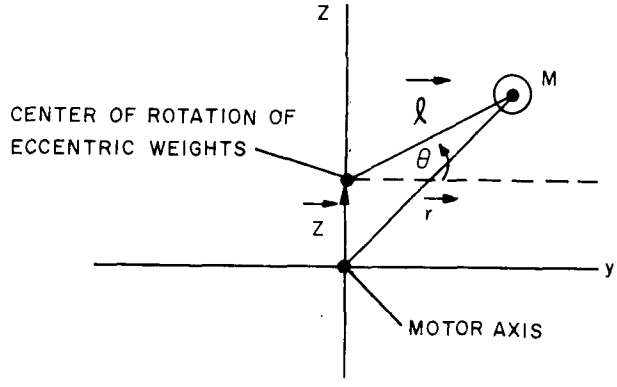

Unit Vectors

$$\vec{e}_y,\ \vec{e}_Z,\ \vec{e}_x$$

then:

$$\vec{\ell} = \vec{e}_Z\, \ell \sin\theta + \vec{e}_y\, \ell \cos\theta \tag{56}$$

and

$$\dot{\vec{\ell}} = \vec{e}_Z \frac{d}{dt}\ell \sin\theta + \vec{e}_y \frac{d}{dt}\ell \cos\theta \tag{57}$$

also

$$\vec{Z} = \vec{e}_Z\,(Z + \ell \sin\theta) \tag{58}$$

and

$$\dot{\vec{Z}} = \vec{e}_Z \frac{d}{dt}(Z + \ell \sin\theta) \tag{59}$$

$$\vec{r} = \vec{Z} + \vec{\ell} \tag{60}$$

$$\dot{\vec{r}} = \dot{\vec{Z}} + \dot{\vec{\ell}} \tag{61}$$

$$\text{Torque} = \frac{d}{dt}(\text{angular momentum})$$

$$\Sigma \vec{T} = \frac{dh}{dt} \tag{62}$$

*This material was reproduced from notes compiled by D. P. Ankeney.

$$\vec{h} = \vec{r} \times m \vec{v} \tag{63}$$

but

$$\frac{d\vec{r}}{dt} = \vec{v} = \dot{\vec{r}} \tag{64}$$

so:

$$\vec{h} = \vec{r} \times m \dot{\vec{r}} \tag{65}$$

sub: 60-61 in 65

$$\vec{h} = (\vec{Z} + \vec{\ell}) \times m (\dot{\vec{Z}} + \dot{\vec{\ell}}) \tag{66}$$

sub: 56-57-58-59 in 66.

$$\vec{h} = m \left[\vec{e}_y \ell \cos\theta + \vec{e}_Z (Z + \ell \sin\theta) \right] \times \left[\frac{\ell d}{dt} \cos\theta + \frac{d}{dt} (Z + \ell \sin\theta) \right] \tag{67}$$

Expressing 62 in determinate form

$$\Sigma \vec{T} = m \frac{d}{dt} \begin{vmatrix} \vec{e}_x & \vec{e}_y & \vec{e}_Z \\ O & \ell \cos\theta & Z + \ell \sin\theta \\ O & \ell \frac{d}{dt} \cos\theta & \frac{d}{dt} (Z + \ell \sin\theta) \end{vmatrix} \tag{68}$$

Solution of determinate yields

$$T = m \frac{d}{dt} \left[\ell \cos\theta \frac{d}{dt} (Z + \ell \sin\theta) - \ell \frac{d}{dt} \cos\theta (Z + \ell \sin\theta) \right] \tag{69}$$

or

$$T = m \ell \left[Z \ddot{\theta} \sin\theta + \ell \ddot{\theta} + (\ddot{Z} + Z \dot{\theta}^2) \cos\theta \right] \tag{70}$$

MOTOR EQUATIONS

Separately excited shunt motor

$$E_m = I_a R_a + K_1 \dot{\theta} \tag{71}$$

$$T = K_1 I_a \text{ (developed torque)} \tag{72}$$

$$T = J \ddot{\theta} + B \dot{\theta} + T_f \text{ (required torque)} \tag{73}$$

JETAVATOR EQUATION

$$F_1 = 10,000 \sin \omega_1 t \qquad (74)$$

Where ω_1 is varied with following waveforms:

sinusoidal 1 to 10 cps
triangular 1 and 2 cps
square 1 cps

DEFINITION OF SYMBOLS

B = Viscous damping coefficient (motor)

C_r & C_f = Viscous damping coefficient (spring-mass-system)

E_m = Terminal voltage (drive motor)

I_a = Armature current (drive motor)

J = Polar moment of inertia (rocket motor)

J = Effective moment of inertia (drive motor)

K_1 = Motor constant (drive motor)

K_r & K_f = Spring constant (spring-mass-system)

ℓ = Effective moment arm (mechanical oscillator)

m = Effective mass (mechanical oscillator)

M = Sprung weight (spring-mass-system)

R_a = Armature resistance (drive motor)

ψ = Angle of rotation (pitching mode)

$\dot{\psi}$ = Angular velocity (pitching mode)

$\ddot{\psi}$ = Angular acceleration (pitching mode)

$\not{z}$ = Vertical displacement (rocket motor)

$\dot{\not{z}}$ = Vertical velocity (rocket motor)

$\ddot{\not{z}}$ = Vertical acceleration (rocket motor)

θ = Angle of rotation (drive motor)

$\dot{\theta}$ = Angular velocity (drive motor)

$\ddot{\theta}$ = Angular acceleration (drive motor)

h = Angular momentum

VARIABLE COEFFICIENTS

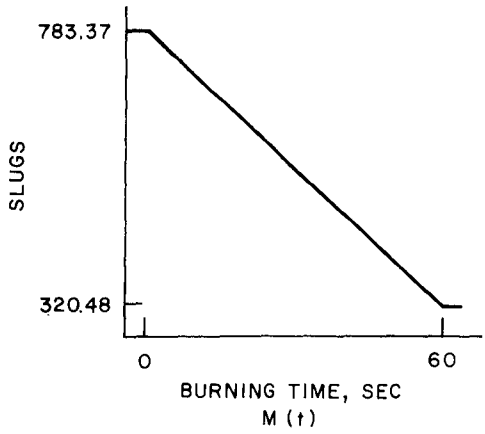

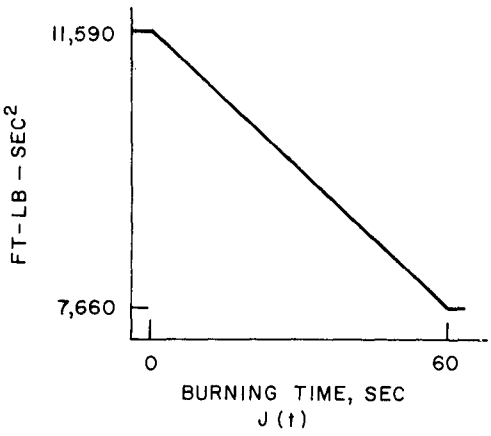

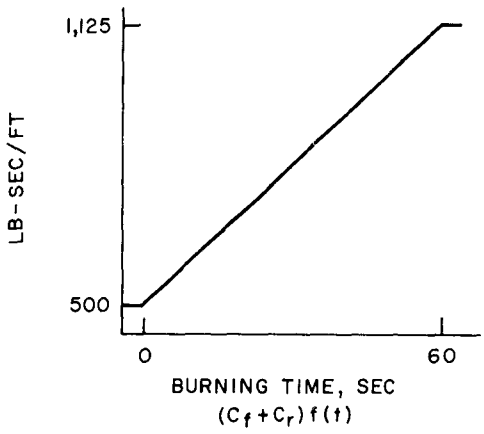

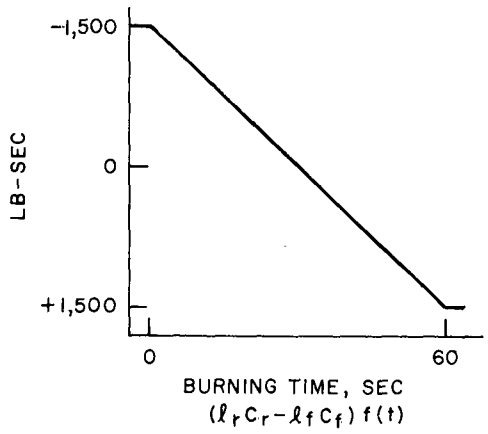

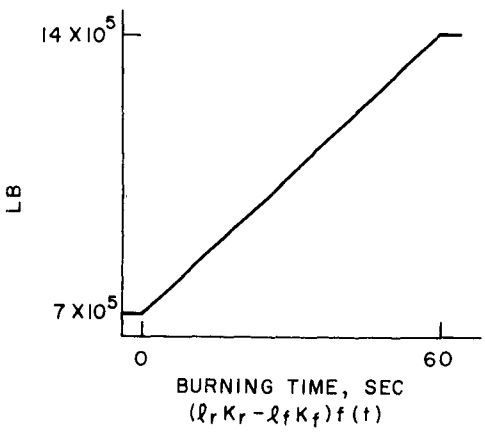

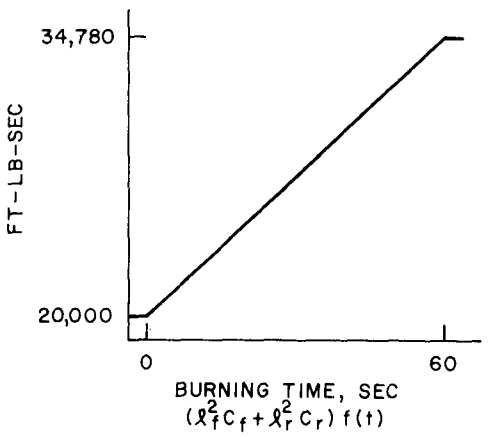

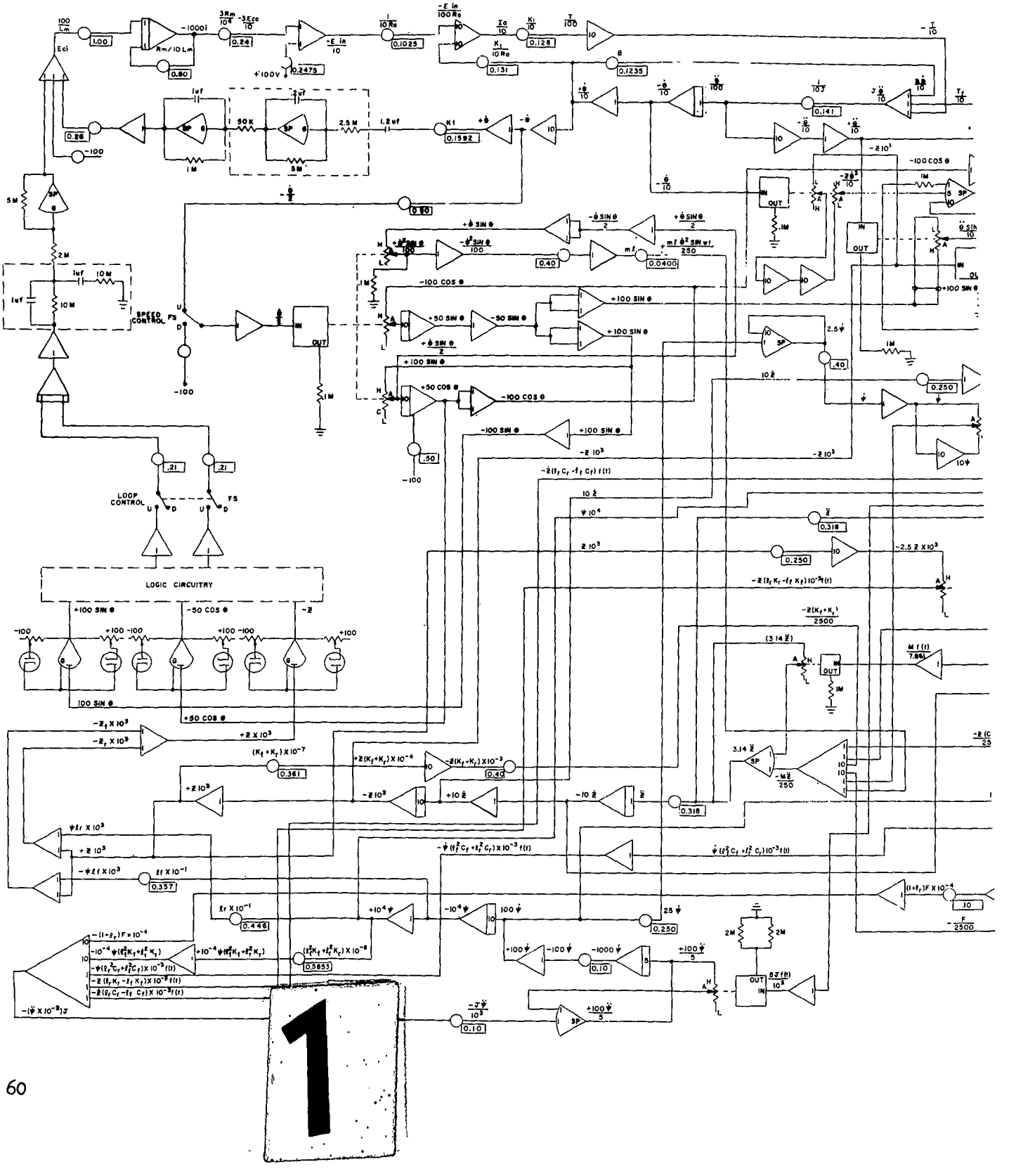
LOOP CONTROL
FS
SPEED CONTROL
LOGIC CIRCUITRY
+100 SIN θ
-50 COS θ
-Ż
100 SIN θ
+50 COS θ
1

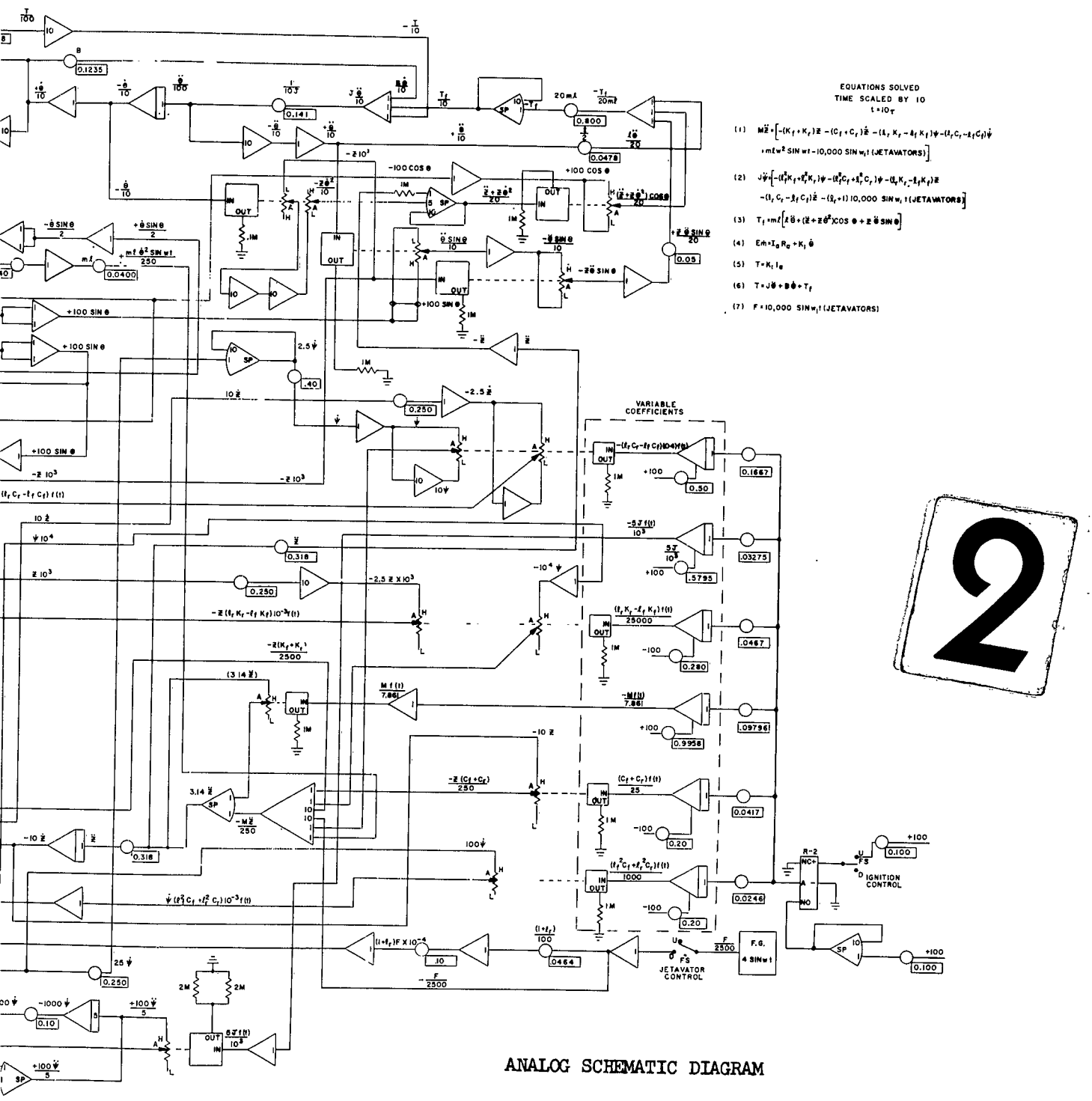

2

ANALOG SCHEMATIC DIAGRAM

Appendix C

DERIVATION OF SYSTEM TRANSFER FUNCTIONS AND PHASE COMPARATOR SCHEMATIC

INTEGRATOR

A high-gain operational amplifier was used in the following configuration to provide the integration indicated in Fig. 7.

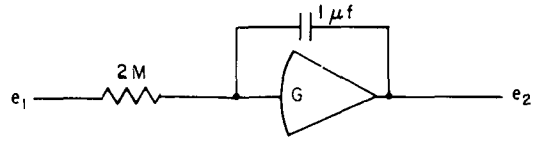

OPERATIONAL AMPLIFIER

The transfer function for an operational amplifier* is given as

$$\frac{e_2}{e_1} = \frac{Z\ f.b.}{Z\ in}$$

where

Z f.b. = feedback impedance

Z in = input impedance

and in LaPlace notation

$$Z\ f.b. = \frac{1}{SC} = \frac{1 \times 10^6}{S}$$

$$Z\ in = 2M$$

then $$\frac{e_2}{e_1} = \frac{1}{2S}$$

and $$K_1 = \frac{1}{2}$$

*Walter J. Karplus and Walter W. Sorous. Analog Methods. New York, McGraw-Hill, 1959. P. 39.

LEAD COMPENSATION

The lead compensation indicated in the forward loop of Fig. 7 has the following configuration:

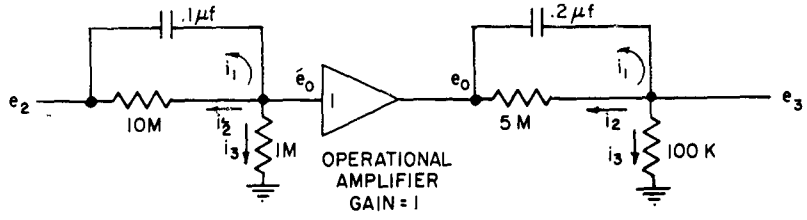

Using nodal analysis:

$$i_1 + i_2 + i_3 = 0$$

and

$$i_1 = \frac{S}{10\ M}\left(e_o - e_2\right)$$

$$i_2 = \frac{e_o - e_2}{10\ M}$$

$$i_3 = \frac{e_o}{1\ M}$$

combining

$$\frac{S}{10\ M}\left(e_o - e_2\right) + \frac{\left(e_o - e_2\right)}{10\ M} + \frac{e_o}{1\ M} = 0$$

rearranging

$$e_o\left(\frac{S}{10\ M} + \frac{1}{10\ M} + \frac{1}{1\ M}\right) = e_2\left(\frac{1}{10\ M} + \frac{S}{10\ M}\right)$$

and

$$\frac{e_o}{e_2} = \frac{(S + 1)}{(S + 11)} \quad ;$$

$\frac{e_3}{e_o}$ is obtained in the same manner and is

$$\frac{e_3}{e_o} = \frac{(S + 1)}{(S + 50)}$$

from which

$$\frac{e_3}{e_2} = \frac{(S + 1)^2}{(S + 11)(S + 50)}$$

MINOR LOOP FEEDBACK

The differentiator and compensation circuitry indicated in the minor loop feedback path of Fig. 7 utilizes an operational amplifier connected as follows:

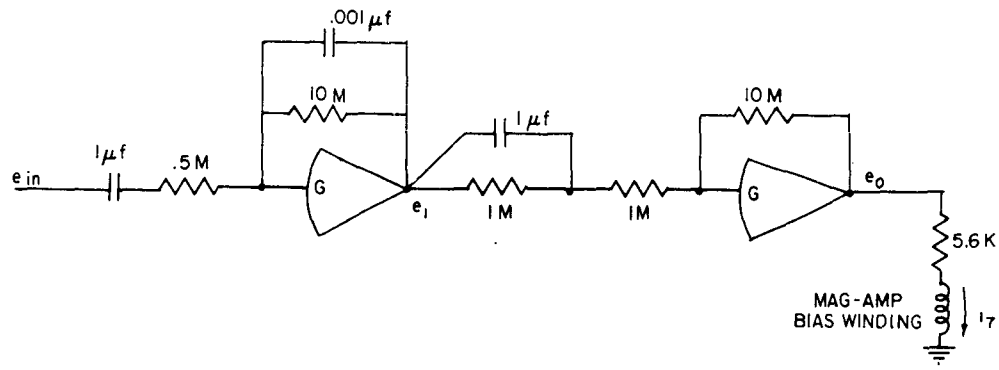

Using the transfer function for operational amplifiers

$$\frac{e_o}{e\ in} = \frac{Z\ f.b.}{Z\ in}$$

It can be shown that the feedback capacitor in the above sketch used for filtering the differentiated ripple of the tachometer output, will contribute a pole in the overall transfer function at S = -100 and as such will not significantly affect the root locus plot. Therefore, the capacitor will not be included in the following derivation:

$$\frac{e_1}{e\ in} = \frac{10\ M}{.5M + \frac{M}{S}} = \frac{20\ S}{(S + 2)}$$

and

$$\frac{e_o}{e_1} = \frac{10\ M}{\frac{M^2}{\frac{M + \triangle\triangle}{S}} + M} = \frac{10\ (S + 1)}{(S + 2)}$$

so that the final transfer function is

$$\frac{e_o}{e\ in} = \frac{e_1}{e\ in} \times \frac{e_o}{e_1}$$

$$\frac{e_o}{e\ in} = \frac{200\ S(S + 1)}{(S + 2)^2}$$

The tachometer constant of 0.3 and the conversion for the 5.6K load resistor gives a final transfer function of

$$\frac{i_7}{\theta} = \frac{10.8 \times 10^{-3}\ S(S + 1)}{(S + 2)^2}$$

$$K_4 = 10.8 \times 10^{-3}$$

PREAMPLIFIER

The preamplifier indicated in Fig. 7 has the following experimentally determined response curve:

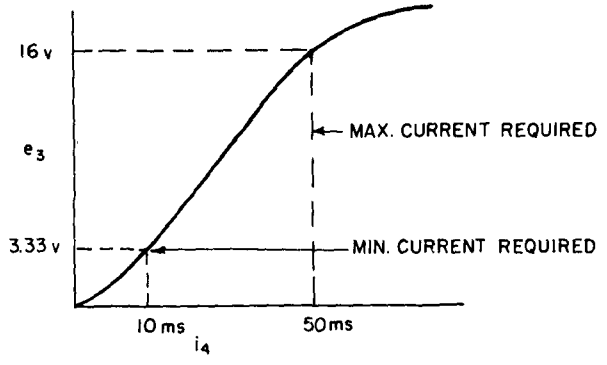

The response characteristic is considered linear over the necessary range of operation. The preamp constant is found to be:

$$\frac{i_4}{e_3} = A_1 = 3 \times 10^{-3}$$

SIGNAL SENSORS

The input signals to the phase comparator were obtained with the use of carbon film potentiometers (see Fig. 31 for approximate hardware location). The sinusoidal signals depicting the driving-function response and the reference response were obtained by attaching a sine-cosine, continuous-turn potentiometer to the rotating shaft of the force generator. The signal depicting the displacement motion was obtained by attaching the sliding arm of a linear-motion potentiometer to the thrust stand leg. Although the sine-cosine unit was adequate in the operation of the experimental system, these units have a relatively short life and should be replaced with electromagnetic devices in the development of an operational system.

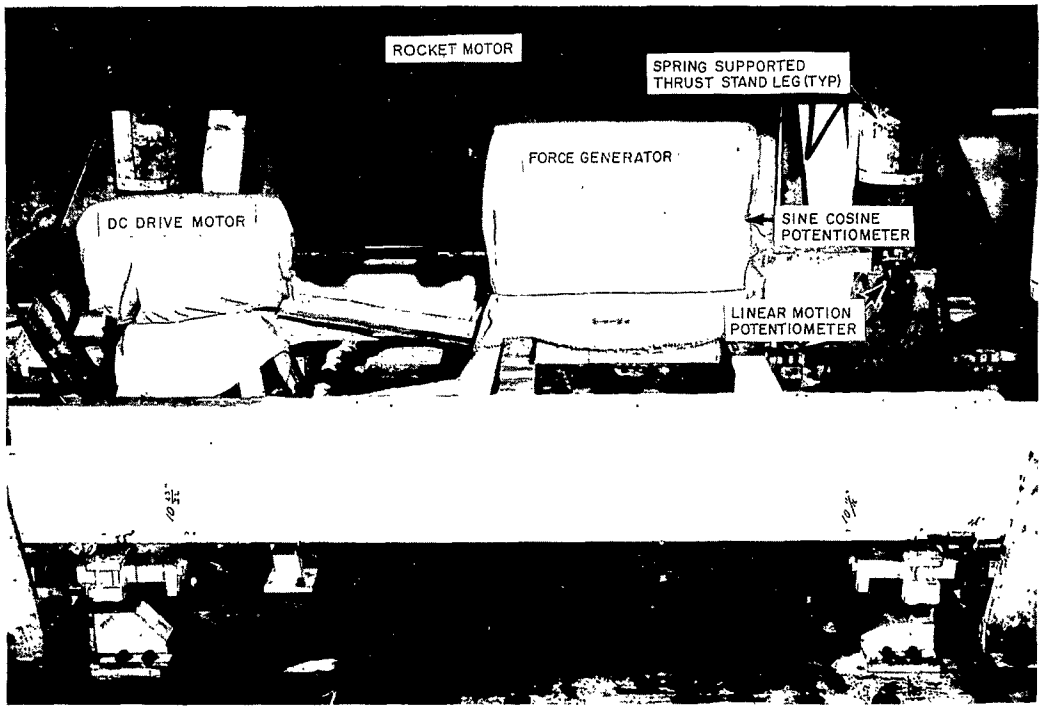

FIG. 31. Large Rocket Motor in Three-Component Stand Prior to Firing.

DC DRIVE MOTOR

The motor constants, R_a, L_a, and K, were determined experimentally using the procedure described in the literature cited below.* The values were found to be:

$$R_a = .86 \text{ ohms}$$

$$L_a = 4 \ \mu h \text{ (negligible)}$$

$$K = 1.68 \ \frac{\text{ohm-second}}{\text{radian}}$$

The inertia was listed by the manufacturer for the motor and was calculated for the force generator. The total inertia is

$$J = .71 \text{ ft-lb-sec}^2$$

The motor time constant is defined as

$$\tau_m = \frac{R_a J}{K^2}$$

and is $\tau_m = .1$ seconds

Since $1/\tau_m$ positions the pole in the motor transfer function, the following expression is obtained, neglecting L_a:

$$\frac{\theta}{e_6} = \frac{10}{S\,(S + 10)}$$

MAGNETIC AMPLIFIER

The steady-state response curve of the magnetic amplifier and drive motor was determined as a single unit under operating conditions, see page 20. The transient response characteristic of the magnetic amplifier was determined experimentally as shown in the following sketch:

*Office of Chief of Ordnance, Department of the Army. Servomechanisms, Section 4, Power Elements and System Design. August 1959. (ORDP 20-139).

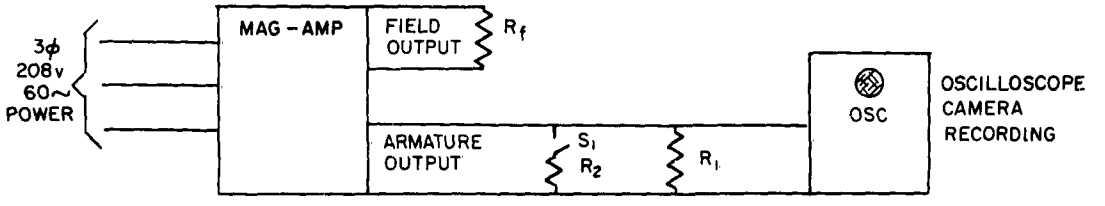

In the above setup the fixed resistance R_f is connected to the field output terminals of the amplifier to simulate the field of the drive motor. The resistance R_1 simulates the motor armature load. An appropriate resistance was chosen to correspond to 1/2 full load. With the mag-amp energized the switch S_1 was closed. The load of R_2 is then added to that of R_1. The resulting transient was recorded and is interpolated below.

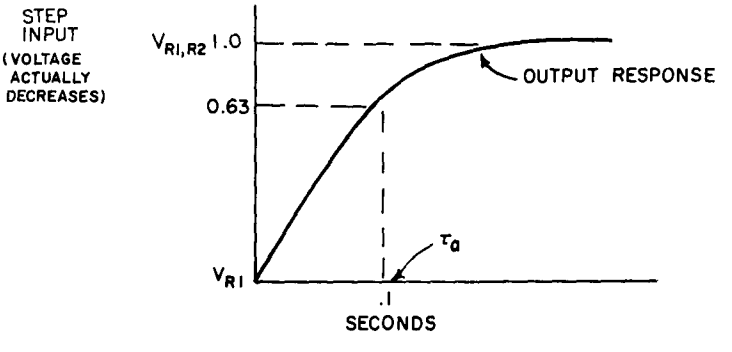

The response curve approaches that of an exponential resulting from a pure R, L circuit having a time constant of 0.1 seconds. Thus, the transfer function is

$$\frac{e_6}{i_5} = \frac{A_2}{(S + 1/\tau_a)} = \frac{A_2}{(S + 10)}$$

A_2 is determined from steady-state characteristics as described on page 20.

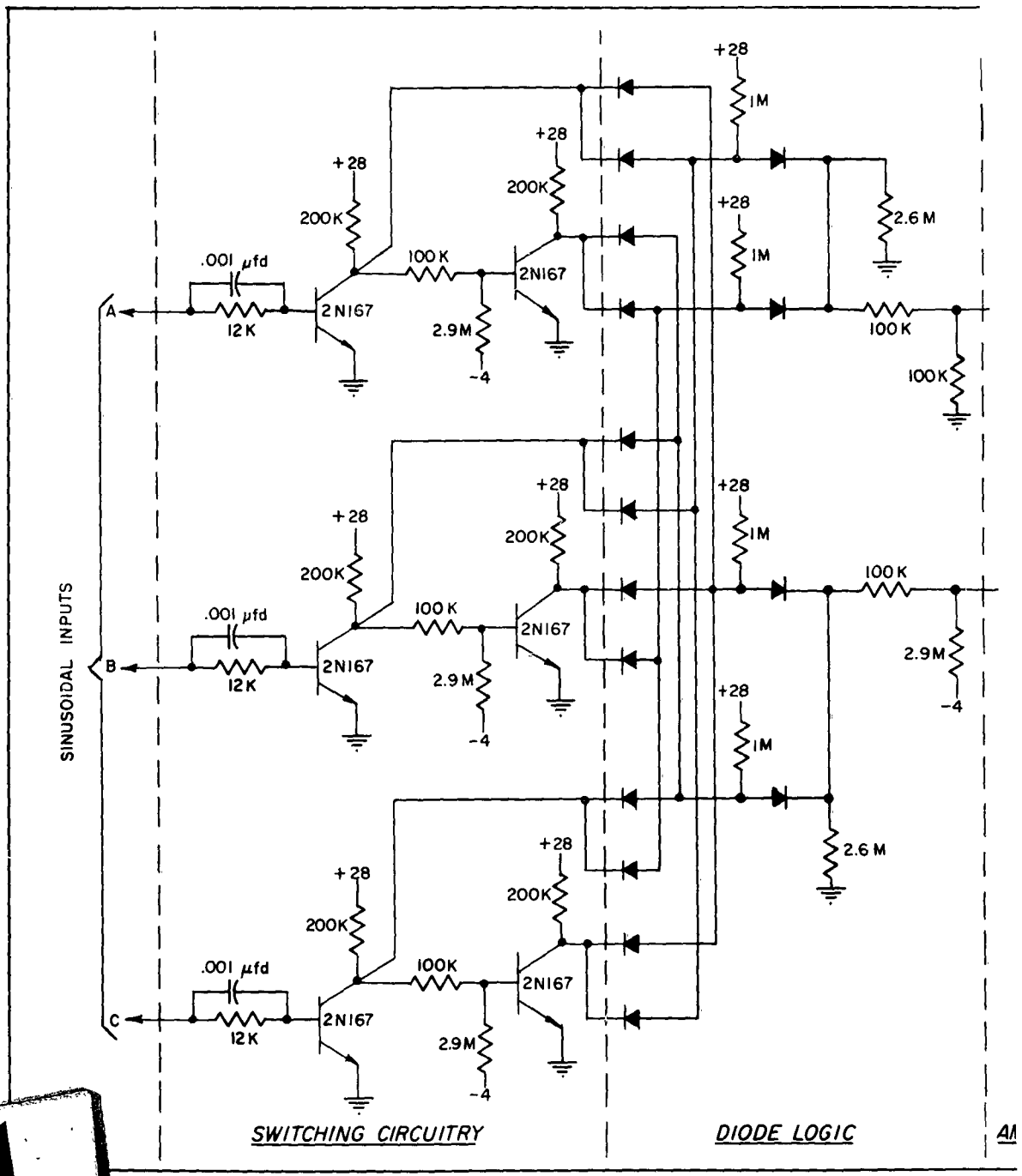
SINUSOIDAL INPUTS
A
B
C
+28
200K
.001 μfd
12K
2N167
100K
2.9M
-4
1M
2.6M
100K
SWITCHING CIRCUITRY
DIODE LOGIC

1

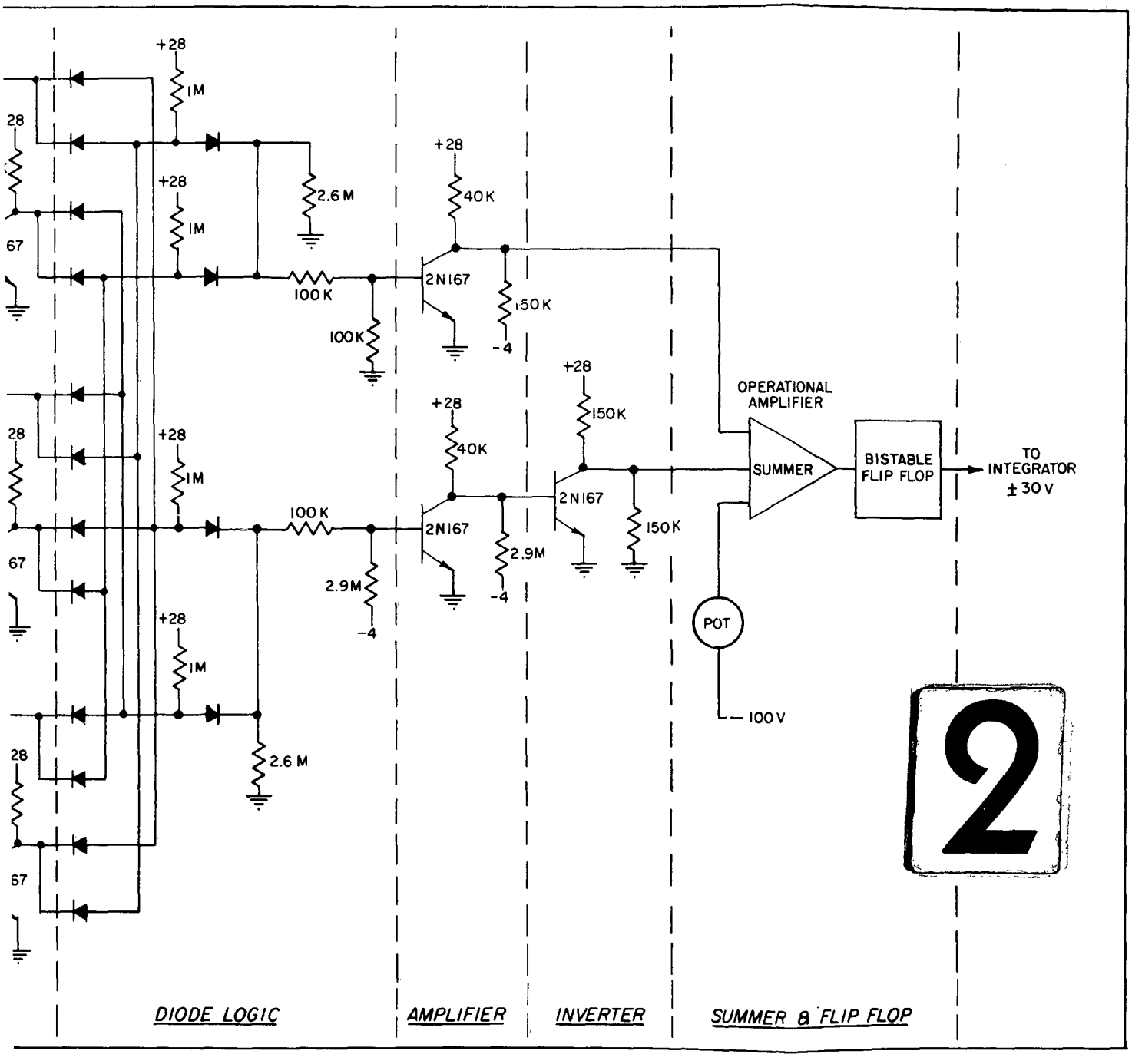
+28
1M
28
67
2.6 M
100 K
2N167
40K
150K
-4
OPERATIONAL AMPLIFIER
SUMMER
BISTABLE FLIP FLOP
TO INTEGRATOR ±30 V
2.9M
POT
100 V
DIODE LOGIC
AMPLIFIER
INVERTER
SUMMER & FLIP FLOP

BIBLIOGRAPHY

Chestnut, Harold and Robert W. Mayer. Servomechanisms and Regulating System Design, Vol. I. New York, Wiley, 1961.

------. Servomechanisms and Regulating System Design. Vol. II. New York, Wiley, 1956.

Cosgriff, Robert Lien. Nonlinear Control Systems. New York, McGraw-Hill, 1958.

Gardner, Murray F. and John L. Barnes. Transients in Linear Systems, Vol. I. New York, Wiley, 1956.

Karplus, Walter J. and Walter W. Sorous. Analog Methods. New York, McGraw-Hill, 1959.

Office of Chief of Ordnance, Department of the Army. Servomechanisms, Section 4, Power Elements and System Design. August 1959. (ORDP 20-139).

Savant, C. J. Basic Feedback Control System Design. New York, McGraw-Hill, 1958.

Thaler, G. J. and R. G. Brown. Servomechanism Analysis. New York, McGraw-Hill, 1953.

Thaler, G. J. and Marvin P. Pastel. Analysis and Design of Nonlinear Feedback Control Systems. New York, McGraw-Hill, 1962.

U. S. Naval Ordnance Test Station. A System for Correcting for Spurious Natural-Frequency Ringing of Rocket Static Thrust Stands, by J. S. Ward. China Lake, Calif., NOTS, 1 September 1960. (NAVWEPS Report 7569, NOTS TP 2541).

------. Determination of Rocket-Motor Mass by Measurement of the Natural Frequency of a Mass-Spring System, by Benjamin Glatt. China Lake, Calif., NOTS, 15 June 1961. (NAVWEPS Report 7741, NOTS TP 2706).

------. Design Cirteria for Large Accurate Solid-Propellant Static-Thrust Stands, by D. P. Ankeney and C. E. Woods. China Lake, Calif., NOTS, June 1963. (NAVWEPS Report 8353, NOTS TP 3240).

ABSTRACT CARD

U. S. Naval Ordnance Test Station
Description of a Control System for Rocket-Motor Mass Measurement, by R. A. Elston. China Lake, Calif., NOTS, June 1963. 70 pp. (NAVWEPS Report 8354, NOTS TP 3241), UNCLASSIFIED.

ABSTRACT. A technique for determining the mass of large rocket motors during burning, and an experimental system developed for use with the NOTS-designed three-component static-test stand at the Skytop facility, are described. The technique involves mounting the rocket motor on springs and continuously exciting

(Over)
1 card, 4 copies

U. S. Naval Ordnance Test Station
Description of a Control System for Rocket-Motor Mass Measurement, by R. A. Elston. China Lake, Calif., NOTS, June 1963. 70 pp. (NAVWEPS Report 8354, NOTS TP 3241), UNCLASSIFIED.
ABSTRACT. A technique for determining the mass of large rocket motors during burning, and an experimental system developed for use with the NOTS-designed three-component static-test stand at the Skytop facility, are described. The technique involves mounting the rocket motor on springs and continuously exciting
(Over)
1 card, 4 copies

U. S. Naval Ordnance Test Station
Description of a Control System for Rocket-Motor Mass Measurement, by R. A. Elston. China Lake, Calif., NOTS, June 1963. 70 pp. (NAVWEPS Report 8354, NOTS TP 3241), UNCLASSIFIED.
ABSTRACT. A technique for determining the mass of large rocket motors during burning, and an experimental system developed for use with the NOTS-designed three-component static-test stand at the Skytop facility, are described. The technique involves mounting the rocket motor on springs and continuously exciting
(Over)
1 card, 4 copies

U. S. Naval Ordnance Test Station
Description of a Control System for Rocket-Motor Mass Measurement, by R. A. Elston. China Lake, Calif., NOTS, June 1963. 70 pp. (NAVWEPS Report 8354, NOTS TP 3241), UNCLASSIFIED.
ABSTRACT. A technique for determining the mass of large rocket motors during burning, and an experimental system developed for use with the NOTS-designed three-component static-test stand at the Skytop facility, are described. The technique involves mounting the rocket motor on springs and continuously exciting
(Over)
1 card, 4 copies

the spring-mass system at its natural frequency.

The theoretical design of the control system is discussed and theoretical system-performance characteristics are compared with those of the experimental system. Results of an analog simulation study conducted in two degrees of freedom are included in the appendix.

Analysis of data from an evaluation test involving the static firing of a large rocket motor, indicates that a 2% accuracy in mass measurement is attainable with the experimental system. Criteria for the design of an operational system that will produce an accuracy of 1% are presented.

NAVWEPS REPORT 8354

the spring-mass system at its natural frequency.

The theoretical design of the control system is discussed and theoretical system-performance characteristics are compared with those of the experimental system. Results of an analog simulation study conducted in two degrees of freedom are included in the appendix.

Analysis of data from an evaluation test involving the static firing of a large rocket motor, indicates that a 2% accuracy in mass measurement is attainable with the experimental system. Criteria for the design of an operational system that will produce an accuracy of 1% are presented.

NAVWEPS REPORT 8354

the spring-mass system at its natural frequency.

The theoretical design of the control system is discussed and theoretical system-performance characteristics are compared with those of the experimental system. Results of an analog simulation study conducted in two degrees of freedom are included in the appendix.

Analysis of data from an evaluation test involving the static firing of a large rocket motor, indicates that a 2% accuracy in mass measurement is attainable with the experimental system. Criteria for the design of an operational system that will produce an accuracy of 1% are presented.

NAVWEPS REPORT 8354

the spring-mass system at its natural frequency.

The theoretical design of the control system is discussed and theoretical system-performance characteristics are compared with those of the experimental system. Results of an analog simulation study conducted in two degrees of freedom are included in the appendix.

Analysis of data from an evaluation test involving the static firing of a large rocket motor, indicates that a 2% accuracy in mass measurement is attainable with the experimental system. Criteria for the design of an operational system that will produce an accuracy of 1% are presented.

INITIAL DISTRIBUTION

9 Chief, Bureau of Naval Weapons
- FWAM (1)
- R-14 (1)
- RM-3 (1)
- RM-35 (1)
- RMMP (1)
- RMMP-12 (1)
- RMMP-241 (1)
- RMMP-4 (1)
- RT (1)

10 Special Projects Office
- Sp-00 (1)
- Sp-01 (1)
- Sp-20 (1)
- Sp-27 (1)
- Sp-271 (3)
- Sp-274 (2)
- Sp-3 (1)

4 Chief of Naval Operations (Operations Evaluation Group)
1 Chief of Naval Research (Code 104)
1 Naval Air Test Center, Patuxent River (Aeronautical Publications Library)
1 Naval Avionics Facility, Indianapolis (Library)
1 Naval Explosive Ordnance Disposal Facility, Naval Propellant Plant, Indian Head
1 Naval Propellant Plant, Indian Head
1 Naval Weapons Evaluation Facility, Kirtland Air Force Base (Code 401)
2 Naval Weapons Services Office
1 Operational Test and Evaluation Force
2 Bureau of Naval Weapons Branch Representative, Cumberland (SPH)
1 Bureau of Naval Weapons Representative, Azusa
3 Bureau of Naval Weapons Representative, Sunnyvale (SPL)
2 Bureau of Naval Weapons Resident Representative, Bacchus (SPLB)
2 Bureau of Naval Weapons Resident Representative, Sacramento (SPLA)
1 Air Force Cambridge Research Laboratories, Laurence G. Hanscom Field
1 Air Force Flight Test Center, Edwards Air Force Base
1 Air Proving Ground Center, Eglin Air Force Base
1 Arnold Engineering Development Center, Tullahoma
2 National Aeronautics and Space Administration
- R. Ziem (1)
- W. Cohen (1)

1 Allegany Ballistics Laboratory, Cumberland
1 Bruce H. Sage Consultant, Pasadena
1 Hercules Powder Company, Bacchus Works, Bacchus, Utah
1 Inca Engineering Corporation, Pasadena